Cancer Tissue Engineering: development of new 3D models and technologies to support cancer research

Marta Maria Cavo

Doctoral School of Bioengineering and Robotics

Curriculum of Bioengineering and Bioelectronics

XXX Cycle

Supervisors:

Prof. Marco Massimo Fato

Dr. Silvia Scaglione

This dissertation is submitted for the degree of

Doctor of Philosophy

February 13th, 2018

A mia madre e mio padre

Abstract (Italiano)

L'attività di ricerca di questa tesi si concentra sulla rilevanza che modelli appropriati che riproducono il microambiente tumorale in vivo sono essenziali per migliorare le nostre conoscenze sul cancro e per testare nuovi composti antitumorali. I modelli animali hanno dimostrato non essere del tutto compatibili con il sistema umano, e le percentuali di successo tra gli studi su animale e su uomo sono ancora insoddisfacenti. D'altra parte, le colture cellulari 2D non riproducono alcuni aspetti del sistema tumorale. Queste limitazioni hanno un peso significativo soprattutto durante lo screening di nuovi farmaci, poiché è stato dimostrato che le cellule sono meno sensibili ai trattamenti se a contatto con il loro microambiente. Per ottenere gli stessi livelli di inibizione delle cellule tumorali osservati in vivo, l'ambiente di coltura deve dunque riflettere l'ambiente naturale 3D. In questo contesto, idrogel naturali o sintetici hanno riportato risultati positivi nell'imitare l'ambiente ECM.

Durante questo dottorato, ho sviluppato diversi scaffold basati su gel da utilizzare come substrati per la coltura di cellule di cancro al seno. In dettaglio, ho sviluppato diversi gel per linee cellulari tumorali a bassa ed alta aggressività (i.e. MCF-7 e MDA-MB-231), ottenendo risultati significativi per quanto riguarda la riproduzione di caratteristiche chiave normalmente presenti nell'ambiente in vivo. Considerando l'importanza del processo di metastasi nell'evoluzione del cancro al seno, mi sono poi concentrata su un nuovo set-up per l'osservazione della motilità e dell'invasione delle cellule tumorali. In particolare, ho unito un approccio bioingegneristico basato su bioreattore con l'analisi a singola cellula di cellule tumorali circolanti (CTCs). Questa parte del lavoro è stata svolta

presso il Dipartimento di Biomedicina dell'Università di Basilea (CH) che, tra le sue facilities, ha un apparecchio per l'analisi di singole cellule.
Alla fine di questo lavoro, ho fornito una proof-of-concept che l'approccio può funzionare, oltre a dimostrare che le cellule possono essere estratte dal dispositivo e utilizzate per l'analisi molecolare.

Abstract (English)

The activity of research of this thesis focuses on the relevance that appropriate models reproducing the in vivo tumor microenvironment are essential for improving cancer biology knowledge and for testing new anticancer compounds. Animal models are proven not to be entirely compatible with the human system, and the success rates between animal and human studies are still unsatisfactory. On the other hand, 2D cell cultures fail to reproduce some aspects of tumor system. These limitations have a significant weight especially during the screening of novel antitumor drugs, as it was demonstrated that cells are less sensitive to treatments when in contact with their microenvironment. To obtain the same tumor cell inhibition levels observed in vivo, the culture environment has to reflect the 3D natural environment. Natural or synthetic hydrogels reported successful outcomes in mimicking ECM environment.

During this PhD, I developed different gel-based scaffolds to be use as substrates for the culture of breast cancer cells. In detail, I developed different gels for low and highly aggressive cancer cell lines (i.e. MCF-7 and MDA-MB-231), obtaining significant results as regards the reproduction of key features normally present into the in vivo environment. Considering the importance of the metastasis process in breast cancer evolution, I then focused on a new set-up for the observation of cancer cell motility and invasion. In particular, I combined a bioreactor-based bioengineering approach with single cell analysis of Circulating Tumor Cells (CTCs). This part of work was carried out at the Dipartiment of Biomedicine of the University of Basel (CH) that, among its equipment, has a cell celector machine for single cell analysis.

At the end of this work, I provided a proof-of-concept that the approach can

work, as well as evidence that the cells can be extracted from the device and used for molecular analysis.

Contents

Chapter 1

Introduction

1.1 Breast cancer

Cancer is a broad term for a class of diseases characterized by abnormal cells that grow and invade healthy cells in the body. Breast cancer occurs when malignant tumors develop in the breast. Breast cancer is the most common cancer in women across most ethnic groups and one of the leading causes of cancer-related deaths worldwide.

A healthy female breast is made up of 12–20 sections called lobes. Each of these lobes is made up of many smaller lobules, the gland that produces milk in nursing women. Both the lobes and lobules are connected by milk ducts, which act as stems or tubes to carry the milk to the nipple.

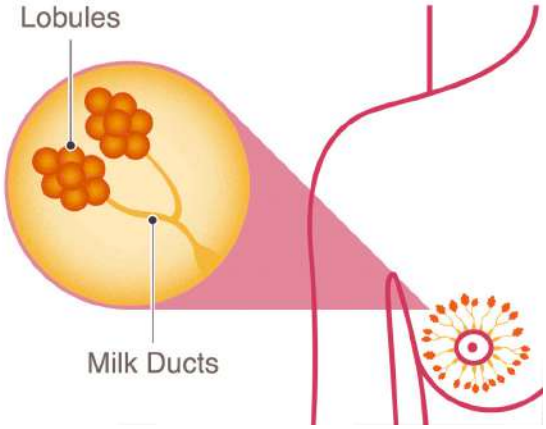

Figure 1.1: Physiology of healthy breast, with lobules and milk ducts.

These breast structures are generally where the cancer begins to form. Cancers developing from the ducts are known as ductal carcinomas, while those developing from lobules are known as lobular carcinomas [1].

Invasive ductal carcinoma (IDC), sometimes called infiltrating ductal carcinoma, is the most common type of breast cancer. About 80% of all breast cancers are invasive ductal carcinomas.

Invasive means that the cancer has "invaded" or spread to the surrounding breast tissues. *Ductal* means that the cancer began in the milk ducts, which are the "pipes" that carry milk from the milk-producing lobules to the nipple. *Carcinoma* refers to any cancer that begins in the skin or other tissues that cover internal organs — such as breast tissue. All together, "invasive ductal carcinoma" refers to cancer that has broken through the wall of the milk duct and begun to invade the tissues of the breast. Over time, invasive ductal carcinoma can spread to the lymph nodes and possibly to other areas of the body.

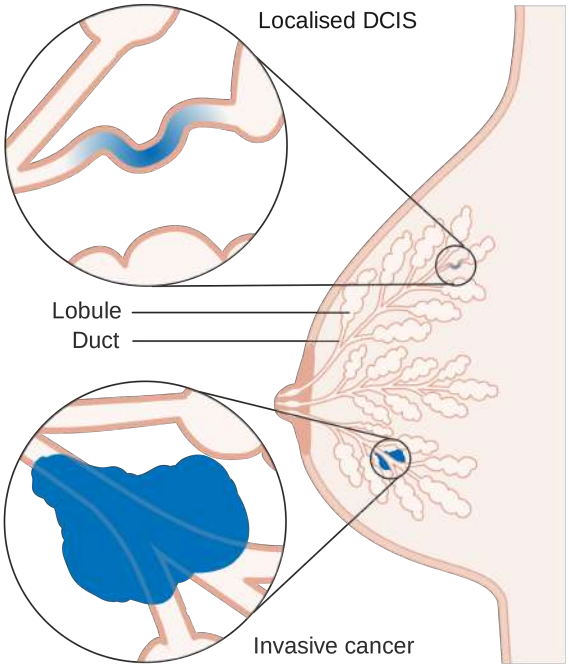

Figure 1.2: Differences between localized DCIS (ductal carcinoma in situ) and invasive cancer.

Most studies divide breast cancer into 4 major molecular subtypes:

- Luminal A
- Luminal B
- Triple negative/basal-like
- HER2 type

Luminal A

Luminal tumor cells look the most like cells of breast cancers that start in the inner (luminal) cells lining the mammary ducts.

Luminal A tumors tend to be:

- Estrogen receptor-positive (ER-positive)
- HER2 receptor-negative (HER2-negative)
- Tumor grade 1 or 2

About 30-70 percent of breast cancers are luminal A tumors.

Of the 4 subtypes, luminal A tumors tend to have the best prognosis, with fairly high survival rates and fairly low recurrence rates.

Luminal B

Luminal B tumors tend to be ER-positive. They may be HER2-negative or HER2-positive. Women with luminal B tumors are often diagnosed at a younger age than those with luminal A tumors.

Compared to luminal A tumors, they also tend to have factors that lead to a poorer prognosis including:

- Poorer tumor grade
- Larger tumor size
- Lymph node-positive

About 10-20 percent of breast cancers are luminal B tumors.

Women with luminal B tumors tend to have fairly high survival rates, although not as high as those with luminal A tumors.

Triple negative/basal-like

Triple negative breast cancers are:

- Estrogen receptor-negative (ER-negative)
- Progesterone receptor-negative (PR-negative)
- HER2-negative

There are several subsets of triple negative breast cancer. One subset is basal-like. Basal-like tumors have cells that look similar to those of the outer (basal) cells surrounding the mammary ducts.

Most triple negative tumors are basal-like and most basal-like tumors are triple negative. However, not all triple negative tumors are basal-like and not all basal-like tumors are triple negative.

About 15-20 percent of breast cancers are triple negative/basal-like. These tumors tend to occur more often in younger women and Black/non-Hispanic black/African-American women (more on race/ethnicity and subtypes of breast cancer). Triple negative/basal-like tumors are often aggressive and have a poorer prognosis compared to the ER-positive subtypes (luminal A and luminal B tumors). However, they can be treated successfully.

HER2 type

About 5-15 percent of breast cancers are HER2 type.

HER2 type tumors tend to be:

- ER-negative
- PR-negative
- Lymph node-positive
- Poorer tumor grade

Women with HER2 type tumors may be diagnosed at a younger age than those with luminal A and luminal B tumors.

HER2 type breast cancers that are HER2-positive can be treated with anti-HER2 drugs such as trastuzumab (Herceptin). Before these drugs were available, HER2 type tumors had a fairly poor prognosis.

1.2. Mechanisms of metastasis

Mortality for breast cancer is more associated to the development of metastases - the spread of a tumor from its primary site to other parts of the body - than to symptoms strictly related to the main lesion [2,3]. Thus, a deeper understanding of the pathways that give rise to metastasis is one of the key challenges for developing new therapies to fight breast cancer [3-5].

Firstly, cancer cells can invade neighbouring healthy tissue. Following this, the cancer cells then invade local lymph nodes or blood vessels.

The inherent characteristics of the lymphatic physiology serve as the primary route for tumor cell metastasis. The increasing size of the tumor triggers a rise in the intratumoral interstitial fluid pressure, and interstitial fluid is released as the system attempts to achieve homeostasis. Unlike the vascular vessels, the lymphatic vessels are highly permeable; the flow rate is approximately 100–500x slower, and coupled with lesser shearing stresses due to vasodilation. Therefore, the lymphatic route is superior in facilitating tumor cell dissemination. Distinguishing between lymphatic endothelial and systemic endothelial cells via immunohistochemical

staining has allowed studies to confirm tumor cell dispersion via afferent lymphatics and lymphangiogenesis, and implicates the lymphatics as the most significant metastatic route.

Metastasis is a complex and inefficient process, which requires sequential regulation of a number of biological steps prior to the presentation of overt disease. This involves tumor cell dissociation, angiogenesis of the primary tumor, intravasation, survival and diffusion through the systemic and lymphatic circulation, adhesion to organ walls, extravasation, establishment of metastatic foci at the organ parenchyma, and finally, manifestation of clinically apparent metastasis via the generation of secondary tumors.

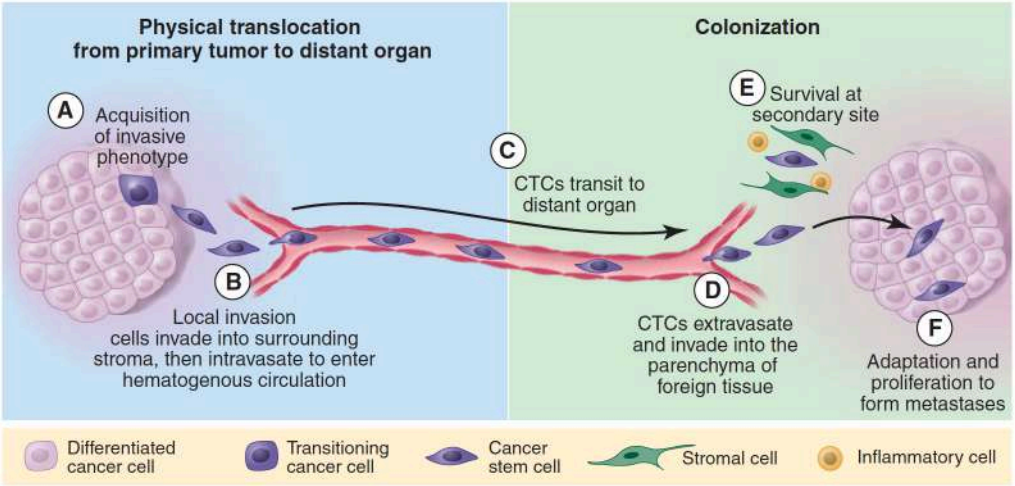

Figure 1.3: Schematic representation of metastasis mechanism

Different sub-processes acting at the cellular level guide each of these steps: several key stages of metastasis - including invasion, intravasation, and extravasation - are thought to involve ExtraCellular Matrix (ECM) degradation and remodelling [6]. Cancer cells contribute to matrix degradation through actin-rich subcellular protrusions known as invadopodia [7]. Invadopodia consists of an actin-rich core surrounded by a number of important protein components, including cytoskeletal

modulators, adhesion proteins, scaffolding proteins, and signaling molecules [8].

A salient aspect of metastasis is the potential of many tumor types to preferentially colonize various organs. Breast cancer cells possess an organ-specific pattern of dissemination and metastasize to bone (47–60%), and subsequently to the liver (19–20%), lung (16–34%), and brain (10–16%). The tumor cells migrate from the primary tumor to the sentinel lymph node. However, no direct lymphatic routes to the preferred target organs have been identified, therefore the tumor cells eventually exit via the efferent lymphatic vessels and utilize the venous system or the nascent blood vessels that serve lymph nodes to merge with the systemic circulation. While this was previously considered to be a passive process, studies have revealed that chemokine receptors C-X-C chemokine receptor type 4 and C-C chemokine receptor type 7 are overexpressed in organs that are primary targets for metastasis (liver, bone and lungs), and may promote migration of their ligands, C-X-C motif chemokine 12/stromal cell-derived factor 1α and chemokine (C-C Motif) ligand 21. Additionally, studies have suggested that the primary tumor secretes vascular endothelial growth factor (VEGF) A and other soluble factors to define a pre-metastatic niche in the target organs, thereby demarcating where the tumor cells should preferentially metastasize.

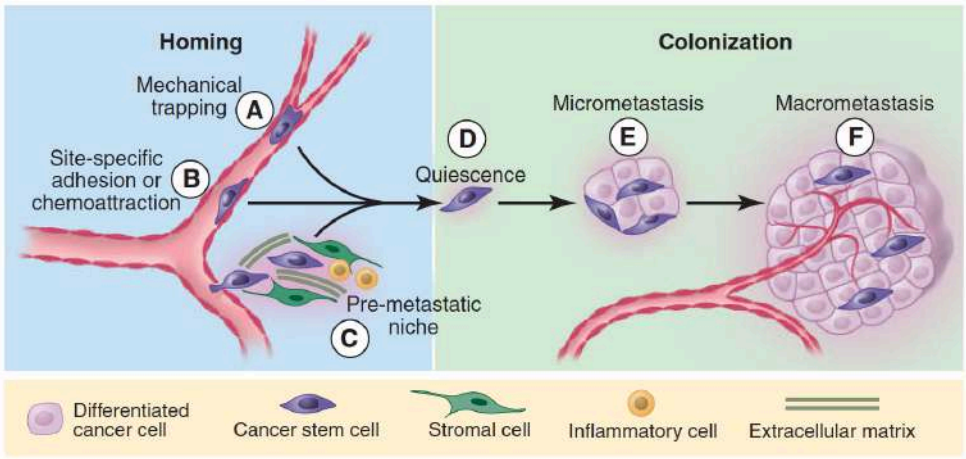

Figure 1.4: Schematic representation of last steps of metastasis: homing and colonization.

1.3. State of the art

1.3.1. 2D models

Traditionally, cancer biology research has involved in vitro analysis of cell behavior predominately using two-dimensional (2D) cell cultures and in vivo animal models [9,10]: in detail, 2D models are routinely used as initial systems for evaluating the effectiveness of molecules as potential therapeutic drugs; this initial screening precedes animal studies before advancing to human clinical trials [11].

The dissimilarities in cell behaviour between 2D cultures and real tumours are well known and they mainly derive from changes in gene expression originated from the different interactions to which cells are subjected within a 2D microenvironment if compared to a more natural 3D [12,13]. A striking example of that is represented by the unequal nutrient concentration to which cells are exposed: in 2D cultures cells are uniformly exposed to nutrients, while in vivo the concentration of soluble factors influencing cell proliferation is characterized by spatial gradients that play a vital role in biological differentiation, organ development and countless other biological processes [14,15].

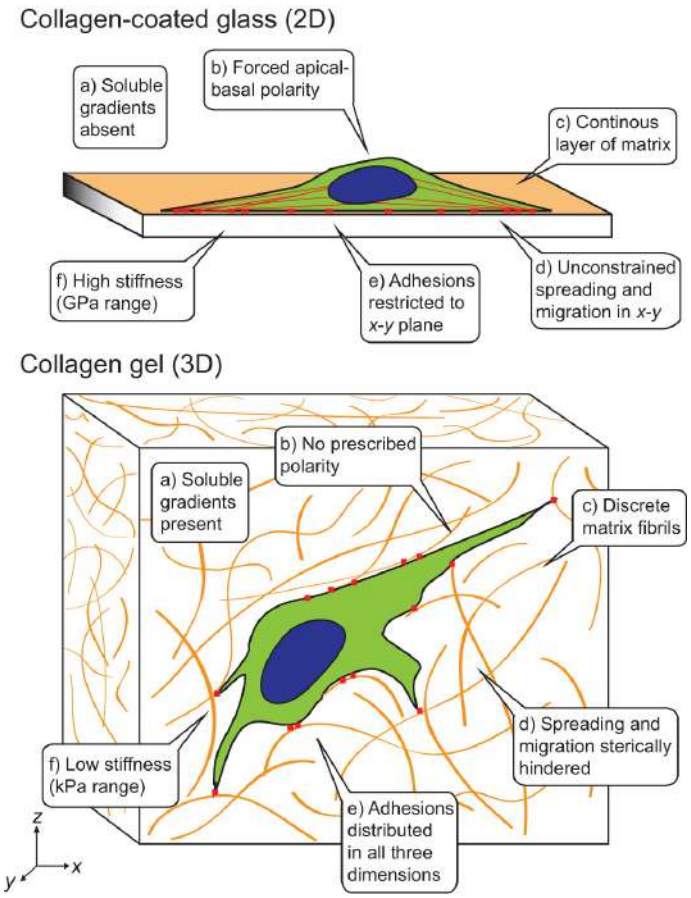

Figure 1.5: Different interactions between cells and substrates (2D versus 3D).

Non-malignant as well as malignant mammary cells have typically been studied as monolayer cultures on tissue culture plastic in the absence of proper ECM thereby losing their tissue-specific function and morphological organization. It is, therefore, not surprising that many aspects of mammary biology and tumorigenesis are still not fully understood.

1.3.2. Animal models

Animal models have not been validated as a necessary step in biomedical research in the scientific literature. Instead, there is a growing awareness of the limitations of animal research and its inability to make reliable predictions for human clinical trials. Indeed, animal studies seem to overestimate by about 30% the likelihood that a treatment will be effective because negative results are often unpublished. Similarly, little more than a

third of highly cited animal research is tested later in human trials. Of the one-third that enter into clinical trials, as little as 8% of drugs pass Phase I successfully.

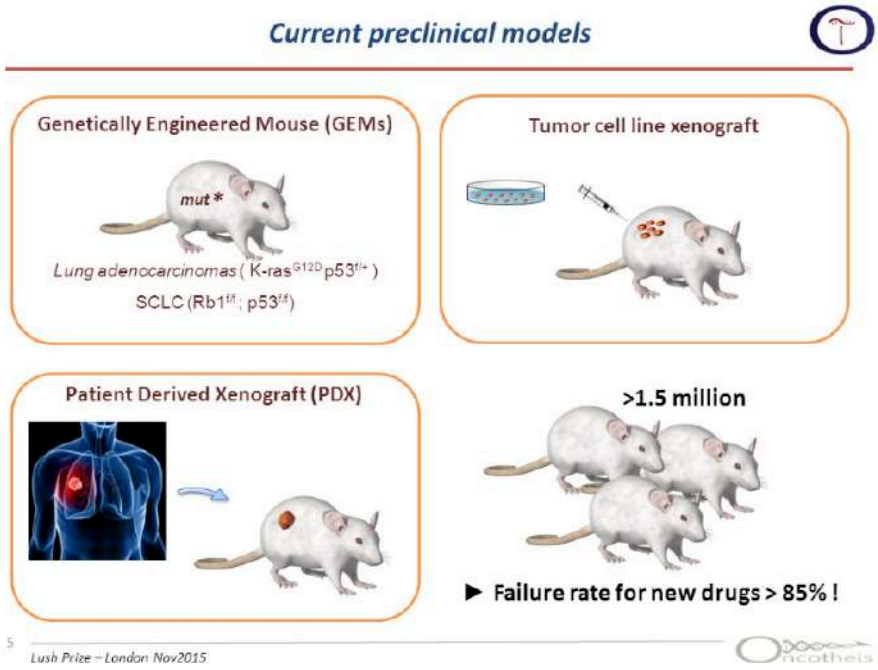

Figure 1.6: Main current preclinical models (in vivo animal models).

The major pre-clinical tools for new-agent screening prior to clinical testing are experimental tumors grown in rodents. Although mice are most commonly used, they are actually poor models for the majority of human diseases. Crucial genetic, molecular, immunologic and cellular differences between humans and mice prevent animal models from serving as effective means to seek for a cancer. Among 4000+ genes in humans and mice, researchers found that transcription factor binding sites differed between the species in 41% to 89% of cases [14].

In many cases, mouse models serve to replicate specific processes or sets of processes within a disease but not the whole spectrum of physiological changes that occur in humans in the disease setting [15].

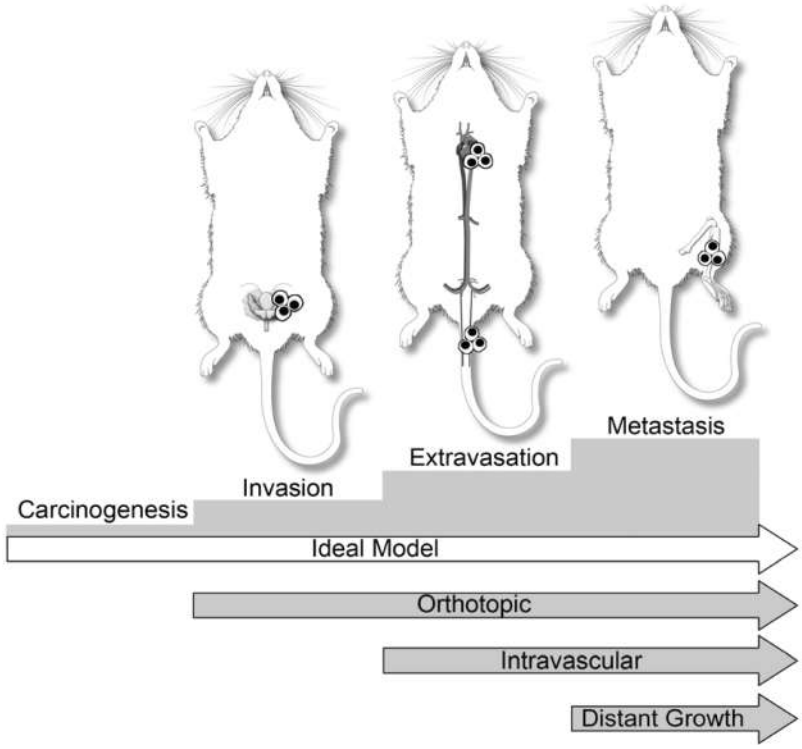

Figure 1.7: Different steps of cancer process that should be modeled in an ideal model (white arrow), versus processes actually modeled by real models (gray arrows).

The failure to translate from animals to humans is likely due in part to poor methodology and failure of the models to accurately mimic the human disease condition. The core of the problem may be rooted in the animal modeling itself. Unlike in human clinical trials, no best-practice standards exist for animal testing [14]. Moreover, the laboratory environment can have a significant effect on experimental results, as stress is a common factor in caged mice [16]. It has been recommended that therapeutic agents should not only be evaluated in rodents, but also in higher animal species, and that randomization and outcomes assessor blinding should be performed. In addition, experiments should be designed in both genders and in different age groups of animals and all data, both positive and negative, should be published [3].

Despite the general lack of success in translating animal models to clinical studies, animals are still prevalently used in laboratories all over the world to test the safety, toxicity and effectiveness of drugs [17]. Animal

models have been essential in cancer research for obvious practical and ethical concerns associated with human experimentation. Animal research is similar to *in vitro* assays, epidemiological investigations, and computer simulations. All attempt to derive probabilistic knowledge in one context that will generalize to humans. All are forms of modeling that will map onto the whole population with less than perfect precision and predict with even less precision the fate of any individual. Notwithstanding, these methods risk missing some important knowledge, or risk finding knowledge that doesn't hold up in the clinical setting even to a point that is actually harmful once widely deployed.

1.3.3. Alternative in vitro models

A wide range of alternatives to animal-based preclinical research has emerged. These include epidemiological studies, autopsies, *in vitro* studies, *in silico* computer modelling, "human organs on a chip" - creating living systems on chips by mimicking a micro-biological environment with cells of a certain organ implanted onto silicon and plastic chips [18], and "microfluidic chips" - automation of over a hundred cell cultures or other experiments on a tiny rubbery silicone integrated circuit with miniscule plumbing [19]. The National Institutes of Health of the United States suspended all new grants for biomedical and behavioural research on chimpanzees after an expert committee concluded that such research was unnecessary [20]. Furthermore, the US National Research Council recommends that animal model based tests be replaced as soon as possible with *in vitro* human cell-based assays, *in silico* models, and an increased emphasis on epidemiology [21]. Of particular interest in this context are the alternative in vitro models, in detail 3D cell cultures and microengineering technologies.

3D cell culture

To understand fully how tissues form and function, as well as their pathophysiology, it is crucial to study how cells and tissues behave as parts of whole living organs that are composed of multiple, tightly opposed tissue types that are highly dynamic and variable in terms of their 3D structure, mechanical properties and biochemical microenvironment. Unfortunately, most studies on cell and tissue regulation have relied on analysis of cells grown in 2D cell-culture models that fail to reconstitute the in vivo cellular microenvironment; as a result, these cultures commonly do not maintain their differentiated functions.

Efforts to address these limitations led to the development of 3D cell-culture models in which cells are grown within extracellular matrix (ECM) gels. This approach enhances expression of differentiated functions and improves tissue organization [1]. Nevertheless, even the most impressive 3D culture models fail to reconstitute features of living organs that are crucial for their function, including tissue–tissue interfaces (e.g. between epithelium and vascular endothelium), spatiotemporal gradients of chemicals and oxygen, and the mechanically active microenvironment that are central to the function of virtually all living organs. Gel-based culture systems also pose major technical challenges in terms of probing effects of physiological diffusion gradients (e.g. ion transport in kidney) or sampling cellular products that are often secreted in a polarized manner (e.g. biliary flow in the liver) because these tissues form in the center of the gel. As a result of these shortcomings of the existing 2D and 3D culture systems, systems-level analysis of cell and disease processes remains largely dependent on time-consuming and costly animal studies. However, as the pharmaceutical industry has come to discover, results obtained in animal experiments often fail to predict human responses.

Microengineering technologies

Development of microengineering approaches has opened entirely new possibilities to create in vitro models that reconstitute more complex 3D organ-level structures and to integrate crucial dynamic mechanical cues as

well as chemical signals. To study polarized functions of various epithelial cells (e.g. intestine, lung, kidney, cornea), for example, two PDMS cell-culture chambers were stacked and separated by a permeable synthetic membrane or ECM. A similar approach has been used to integrate liver epithelium with microfabricated vascular networks [22], and fibroblasts were included as well in another liver model [23]. In this manner, microfabrication was leveraged to reconstitute a tissue–tissue interface that is a crucial element of whole liver organ structure, which was not previously possible in conventional 3D ECM gel cultures.

Replica-molding techniques also have been used to replicate complex surface relief patterns to produce biomimetic structures that mimic organ-specific microarchitecture. Microfabricated structures were built within microfluidic channels that resemble the endothelium that separates hepatocytes from the liver sinusoid in whole liver, with the goal of more closely approximating the mass transport properties of the hepatic microcirculation [24]. This bioinspired liver-on-a-chip enabled primary human hepatocytes to maintain liver-specific met- abolic activity for one week in culture without exogenous ECM coatings, and it induced formation of hepatic cord-like structures with functional bile canaliculi [25]. An array of PDMS microchambers interconnected by narrow (1 mm wide) channels was similarly used to enable growth and in vivo-like reorganization of osteocytes in a 3D environment that replicates the lacuna–canalicular network of bone [26]. Other examples include a compartmentalized microfluidic system that enables co-culture of neurons and oligodendrocytes to study neuron–glia communication during develop-ment of the central nervous system [27] and a microdevice incorporating ECM gels microinjected between two parallel microchannels to investigate the vascularization of liver tissues in 3D culture microenvironments [28].

Similar microsystems approaches have been used to develop disease models. For example, a microfluidic co-culture platform was developed that allows for communication between different tissue types through 3D ECM gels to examine capillary-cell invasion and sprouting in response to

malignant breast and brain tumors [29,30] or behavior of breast cancer cells during the transition of ductal carcinoma in situ to invasive carcinoma [31].

A device incorporating two stacked PDMS microchannel layers separated by a thin porous membrane was used to form heterotypic multicellular spheroids in a 3D microfluidic culture system [32,33] that recapitulates the tumor micro- environment of metastatic prostate cancer cells [34]. A similar strategy permitted study of intravascular adhesion of circulating metastatic breast cancer cells in response to endothelial activation under physiological flow conditions [35]. Using this model, basal stimulation of the endothelium with the cytokine, CXCL12, was shown to significantly increase adhesion of circulating breast cancer cells.

Importantly, microengineering also can be used to mimic the complex biochemical microenvironment of living organs. A microfluidic perfusion bioreactor was constructed to impose oxygen gradients on hepatocytes co-cultured with fibroblasts to mimic physiological variations in hepatocyte form and function along the liver sinusoids, known as liver zonation, which is thought to depend on regional variations in oxygenation [36]. This microdevice effectively reconstituted the regional heterogeneity of liver microarchitecture as well as drug-induced zonal hepatotoxicity seen in vivo. A 3D microfluidic device was used to study chemotactic migration of malignant cancer cells under conditions in which cancer cells were precisely positioned relative to ‘source’ and ‘sink’ cells, which pro- duce and scavenge chemokines causing production of shal- lower and more physiological chemokine gradients [37].

More recently, mechanically active microfluidic culture devices have been created that reproduce the dynamic physical forces that are crucial for organ function, as well as for disease development. For example, primary human small airway epithelial cells were cultured in a microfluidic channel and integrated with a computer-controlled, two-phase (air–liquid) microfluidic switching system to mimic the propagation and rupture of liquid plugs that occur during the reopening of collapsed airways that causes mechanical airway injury in obstructive pulmonary disease [38]. This study revealed severe injurious cellular responses to plug propagation

and rupture – and, impressively, these injury events could be detected acoustically in the device as crackling sounds nearly identical to the respiratory ‘crackles’ that physicians listen for through their stethoscopes to detect fluid in the lung.

In a related study, a mechanically actuatable, multilayered, microfluidic device was developed to expose alveolar epithelial tissues to a combination of cyclic wall-stretch and repeated propagation of a moving air–liquid interface that reproduces the complex pathological mechanical forces experienced by alveolar epithelial cells during mechanical ventilation [39]. Quantitative analysis of mechanical cell injury in this ‘alveolus-on-a-chip’ revealed that a combination of solid and fluid mechanical stresses causes significantly more severe cell injury than either alone, supporting clinical observations that alveolar stretch alone is not sufficient to induce ventilator-induced lung injury. Thus, these relatively simple microengineered tissue mod- els offer an in vitro method to mimic some important facets of complex disease processes that depend crucially on 3D organ structure; again, this result could not be obtained using conventional 3D gel cultures.

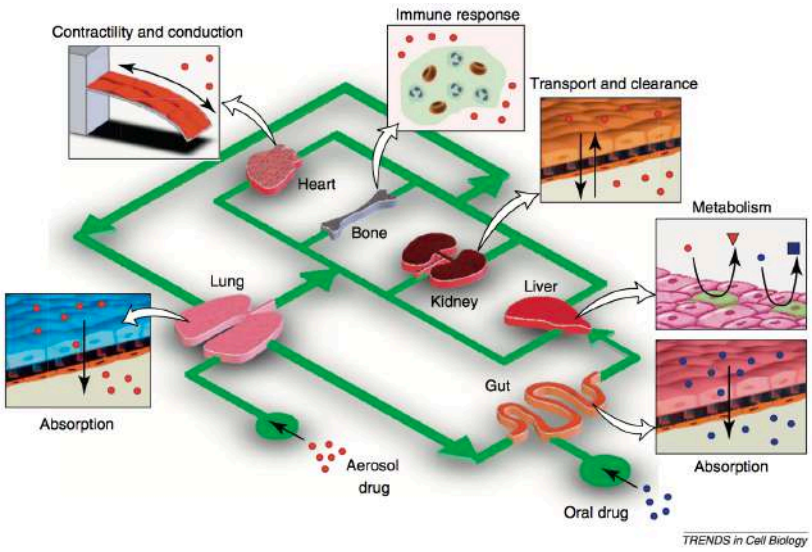

Figure 1.8: The human-on-a-chip concept. Biomimetic microsystems representing different organs can be integrated into a single microdevice and linked by a microfluidic circulatory system.

1.4. Tissue Engineering

The field of tissue engineering (regenerative medicine) aims to repair and regenerate damaged tissues by developing biological substitutes that mimic the natural extracellular matrix to help guide the growth of new functional tissue in vitro or in vivo to restore, maintain or improve tissue function. Tissue engineering technologies are based on a biological triad and involve the successful interaction between three components: (1) the scaffold that holds the cells together to create the tissue's physical form, (2) the cells that synthesise the tissue and (3) signalling mechanisms (i.e. mechanical and chemical signals) that direct the cells to express the desired tissue phenotype [Vacanti, J. P., & Langer, R. (1999). Tissue engineering: the design and fabrication of living replacement devices for surgical reconstruction and transplantation. The lancet, 354, S32-S34.]

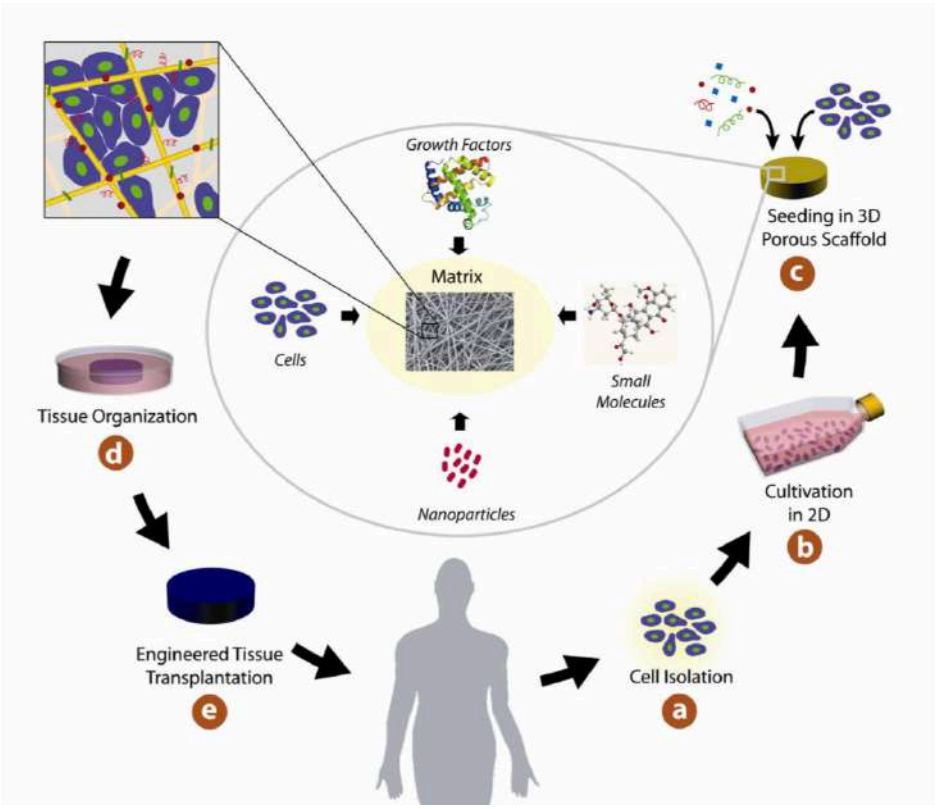

Figure 1.9: Main steps of traditional tissue engineering paradigm.

Bioreactors can be used to provide the signals in this latter area in order to influence biological processes by the application of a mechanical stimulus, and may also be used as an alternative to, or in conjunction with growth factors.

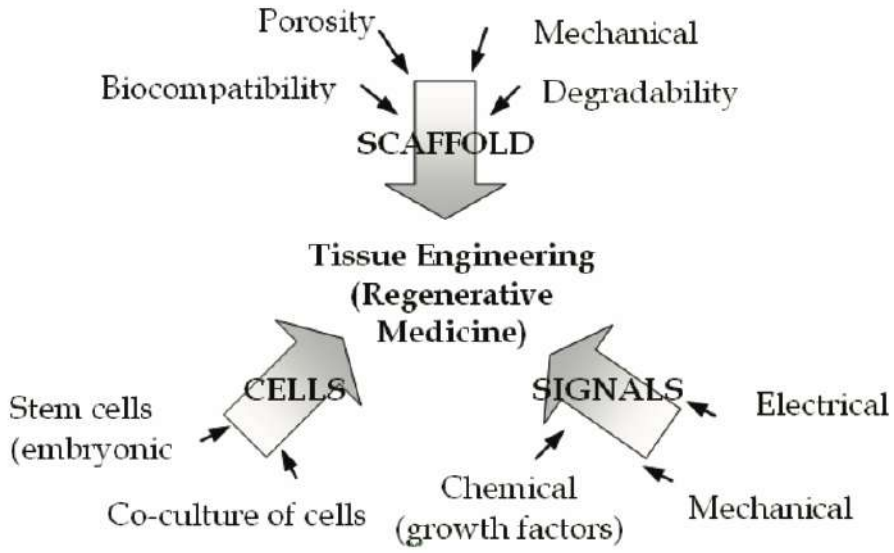

Fig. 1.10: The tissue engineering triad; factors that need to be considered when designing a suitable structure for tissue engineering applications (Lyons, et al., 2008).

1.4.1. Cells

Tissue engineering utilizes living cells as engineering materials. Examples include using living fibroblasts in skin replacement or repair, cartilage repaired with living chondrocytes, or other types of cells used in other ways.

From fluid tissues such as blood, cells are extracted by bulk methods, usually centrifugation or apheresis. From solid tissues, extraction is more difficult. Usually the tissue is minced, and then digested with the enzymes trypsin or collagenase to remove the extracellular matrix (ECM) that holds the cells. After that, the cells are free floating, and extracted using centrifugation or apheresis. Digestion with trypsin is very dependent on temperature: higher temperatures digest the matrix faster, but create more

damage. Collagenase is less temperature dependent, and damages fewer cells, but takes longer and is a more expensive reagent.

Cells are often categorized by their source: *autologous* cells are obtained from the same individual to which they will be reimplanted. Autologous cells have the fewest problems with rejection and pathogen transmission, however in some cases might not be available. For example, in genetic disease suitable autologous cells are not available. Also very ill or elderly persons, as well as patients suffering from severe burns, may not have sufficient quantities of autologous cells to establish useful cell lines. Moreover, since this category of cells needs to be harvested from the patient, there are also some concerns related to the necessity of performing such surgical operations that might lead to donor site infection or chronic pain. Autologous cells also must be cultured from samples before they can be used: this takes time, so autologous solutions may not be very quick.

Allogeneic cells come from the body of a donor of the same species. While there are some ethical constraints to the use of human cells for in vitro studies, the employment of dermal fibroblasts from human foreskin has been demonstrated to be immunologically safe and thus a viable choice for tissue engineering of skin.

Xenogenic cells are these isolated from individuals of another species. In particular animal cells have been used quite extensively in experiments aimed at the construction of cardiovascular implants.

Another distinction is between *primary cells* (derived from an organism) and *cell line* (taken from a cell bank).

Cell line or cell strain may be finite or continuous depending upon whether it has limited culture life span or it is immortal in culture. On the basis of the life span of culture, the cell lines are categorized into two types:

1. Finite cell lines: the cell lines which have a limited life span and go through a limited number of cell generations (usually 20-80 population doublings) are known as finite cell lines. These cell lines exhibit the property of contact inhibition, density limitation

and anchorage dependence. The growth rate is slow and doubling time is around 24-96 hours;

2. Continuous cell lines: cell lines transformed under laboratory conditions or in vitro culture conditions give rise to continuous cell lines. These cell lines show the property of ploidy (aneupliody or heteroploidy), absence of contact inhibition and anchorage dependence. They grow either in a monolayer or in suspension. The growth rate is rapid and doubling time can be 12-24 hours.

1.4.2. Scaffolds

Scaffolds are materials that have been engineered to cause desirable cellular interactions to contribute to the formation of new functional tissues for medical purposes. Cells are often 'seeded' into these structures capable of supporting three-dimensional tissue formation. Scaffolds mimic the extracellular matrix of the native tissue, recapitulating the in vivo milieu and allowing cells to influence their own microenvironments. They usually serve for at least one of the following purposes: allow cell attachment and migration, deliver and retain cells and biochemical factors, enable diffusion of vital cell nutrients and expressed products, exert certain mechanical and biological influences to modify the behaviour of the cell phase.

To achieve the goal of tissue reconstruction, scaffolds must meet some specific requirements. A high porosity and an adequate pore size are necessary to facilitate cell seeding and diffusion throughout the whole structure of both cells and nutrients. Biodegradability is often an essential factor since scaffolds should preferably be absorbed by the surrounding tissues without the necessity of a surgical removal. The rate at which degradation occurs has to coincide as much as possible with the rate of tissue formation: this means that while cells are fabricating their own natural matrix structure around themselves, the scaffold is able to provide structural integrity within the body and eventually it will break down leaving the newly formed tissue which will take over the mechanical load.

Injectability is also important for clinical uses. Recent research on organ printing is showing how crucial a good control of the 3D environment is to ensure reproducibility of experiments and offer better results.

1.4.2.1. Materials

Many different materials (natural and synthetic, biodegradable and permanent) have been investigated. Most of these materials have been known in the medical field before the advent of tissue engineering as a research topic, being already employed as bioresorbable sutures. Examples of these materials are collagen and some polyesters.

New biomaterials have been engineered to have ideal properties and functional customization: injectability, synthetic manufacture, biocompatibility, non-immunogenicity, transparency, nano-scale fibers, low concentration, resorption rates, etc.

A commonly used synthetic material is PLA - polylactic acid. This is a polyester which degrades within the human body to form lactic acid, a naturally occurring chemical which is easily removed from the body. Similar materials are polyglycolic acid (PGA) and polycaprolactone (PCL): their degradation mechanism is similar to that of PLA, but they exhibit respectively a faster and a slower rate of degradation compared to PLA. While these materials have well maintained mechanical strength and structural integrity, they exhibit a hydrophobic nature. This hydrophobicity inhibits their biocompatibility, which makes them less effective for in vivo use as tissue scaffolding. In order to fix the lack of biocompatibility, much research has been done to combine these hydrophobic materials with hydrophilic and more biocompatible hydrogels. While these hydrogels have a superior biocompatibility, they lack the structural integrity of PLA, PCL, and PGA. By combining the two different types of materials, researchers are trying to create a synergistic relationship that produces a more biocompatible tissue scaffolding.

Scaffolds may also be constructed from natural materials: in particular different derivatives of the extracellular matrix have been studied to evaluate their ability to support cell growth. Proteic materials, such as

collagen or fibrin, and polysaccharidic materials, like chitosan[23] or glycosaminoglycans (GAGs), have all proved suitable in terms of cell compatibility, but some issues with potential immunogenicity still remains. Among GAGs hyaluronic acid, possibly in combination with cross linking agents (e.g. glutaraldehyde, water-soluble carbodiimide, etc.), is one of the possible choices as scaffold material. Functionalized groups of scaffolds may be useful in the delivery of small molecules (drugs) to specific tissues. Another form of scaffold under investigation is decellularised tissue extracts whereby the remaining cellular remnants/extracellular matrices act as the scaffold. Recently a range of nanocomposites biomaterials are fabricated by incorporating nanomaterials within polymeric matrix to engineer bioactive scaffolds.

1.4.2.2. Synthesis

A number of different methods have been described in literature for preparing porous structures to be employed as tissue engineering scaffolds. Each of these techniques presents its own advantages, but none are free of drawbacks.

Nanofiber self-assembly

Molecular self-assembly is one of the few methods for creating biomaterials with properties similar in scale and chemistry to that of the natural in vivo extracellular matrix (ECM), a crucial step toward tissue engineering of complex tissues. Moreover, these hydrogel scaffolds have shown superiority in in vivo toxicology and biocompatibility compared to traditional macroscaffolds and animal-derived materials.

Textile technologies

These techniques include all the approaches that have been successfully employed for the preparation of non-woven meshes of different polymers. In particular, non-woven polyglycolide structures have been tested for tissue engineering applications: such fibrous structures have been found

useful to grow different types of cells. The principal drawbacks are related to the difficulties in obtaining high porosity and regular pore size.

Solvent casting and particulate leaching

Solvent casting and particulate leaching (SCPL) allows for the preparation of structures with regular porosity, but with limited thickness. First, the polymer is dissolved into a suitable organic solvent (e.g. polylactic acid could be dissolved into dichloromethane), then the solution is cast into a mold filled with porogen particles. Such porogen can be an inorganic salt like sodium chloride, crystals of saccharose, gelatin spheres or paraffin spheres. The size of the porogen particles will affect the size of the scaffold pores, while the polymer to porogen ratio is directly correlated to the amount of porosity of the final structure. After the polymer solution has been cast the solvent is allowed to fully evaporate, then the composite structure in the mold is immersed in a bath of a liquid suitable for dissolving the porogen: water in the case of sodium chloride, saccharose and gelatin or an aliphatic solvent like hexane for use with paraffin. Once the porogen has been fully dissolved, a porous structure is obtained. Other than the small thickness range that can be obtained, another drawback of SCPL lies in its use of organic solvents which must be fully removed to avoid any possible damage to the cells seeded on the scaffold.

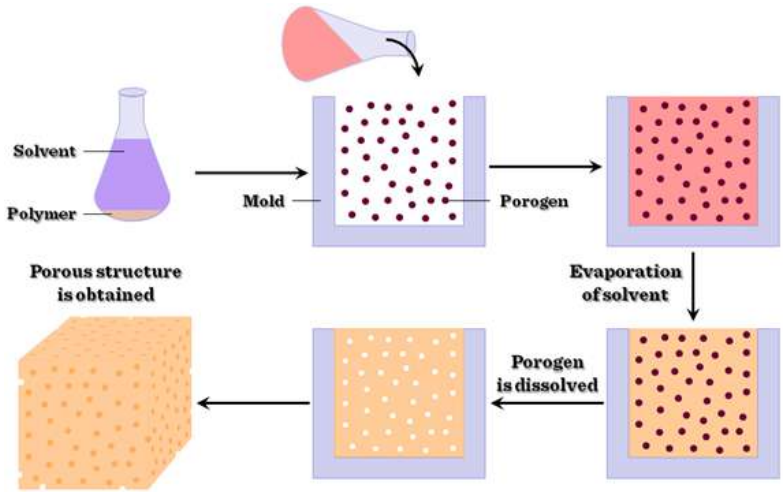

Fig. 1.11: Solvent casting and particulate leaching method for the fabrication of 3D porous scaffolds.

Gas foaming

To overcome the need to use organic solvents and solid porogens, a technique using gas as a porogen has been developed. First, disc-shaped structures made of the desired polymer are prepared by means of compression molding using a heated mold. The discs are then placed in a chamber where they are exposed to high pressure CO2 for several days. The pressure inside the chamber is gradually restored to atmospheric levels. During this procedure the pores are formed by the carbon dioxide molecules that abandon the polymer, resulting in a sponge-like structure. The main problems resulting from such a technique are caused by the excessive heat used during compression molding (which prohibits the incorporation of any temperature labile material into the polymer matrix) and by the fact that the pores do not form an interconnected structure.

Emulsification freeze-drying

This technique does not require the use of a solid porogen like SCPL. First, a synthetic polymer is dissolved into a suitable solvent (e.g. polylactic acid in dichloromethane) then water is added to the polymeric solution and the two liquids are mixed in order to obtain an emulsion. Before the two phases can separate, the emulsion is cast into a mold and quickly frozen by means of immersion into liquid nitrogen. The frozen emulsion is subsequently freeze-dried to remove the dispersed water and the solvent, thus leaving a solidified, porous polymeric structure. While emulsification and freeze-drying allow for a faster preparation when compared to SCPL (since it does not require a time consuming leaching step), it still requires the use of solvents. Moreover, pore size is relatively small and porosity is often irregular. Freeze-drying by itself is also a commonly employed technique for the fabrication of scaffolds. In particular, it is used to prepare collagen sponges: collagen is dissolved into acidic solutions of acetic acid or hydrochloric acid that are cast into a mold, frozen with liquid nitrogen and then lyophilized.

Thermally induced phase separation

Similar to the previous technique, the TIPS phase separation procedure requires the use of a solvent with a low melting point that is easy to sublime. For example, dioxane could be used to dissolve polylactic acid, then phase separation is induced through the addition of a small quantity of water: a polymer-rich and a polymer-poor phase are formed. Following cooling below the solvent melting point and some days of vacuum-drying to sublime the solvent, a porous scaffold is obtained. Liquid-liquid phase separation presents the same drawbacks of emulsification/freeze-drying.

Electrospinning

Electrospinning is a highly versatile technique that can be used to produce continuous fibers from submicrometer to nanometer diameters. In a typical electrospinning set-up, a solution is fed through a spinneret and a high voltage is applied to the tip. The buildup of electrostatic repulsion within the charged solution, causes it to eject a thin fibrous stream. A mounted collector plate or rod with an opposite or grounded charge draws in the continuous fibers, which arrive to form a highly porous network. The primary advantages of this technique are its simplicity and ease of variation. At a laboratory level, a typical electrospinning set-up only requires a high voltage power supply (up to 30 kV), a syringe, a flat tip needle and a conducting collector. For these reasons, electrospinning has become a common method of scaffold manufacture in many labs. By modifying variables such as the distance to collector, magnitude of applied voltage, or solution flow rate—researchers can dramatically change the overall scaffold architecture.

Historically, research on electrospun fibrous scaffolds dates back to at least the late 1980s when Simon showed that electrospinning could be used to produced nano- and submicron-scale fibrous scaffolds from polymer solutions specifically intended for use as in vitro cell and tissue substrates. This early use of electrospun lattices for cell culture and tissue engineering showed that various cell types would adhere to and proliferate upon polycarbonate fibers. It was noted that as opposed to the flattened

morphology typically seen in 2D culture, cells grown on the electrospun fibers exhibited a more rounded 3-dimensional morphology generally observed of tissues in vivo.

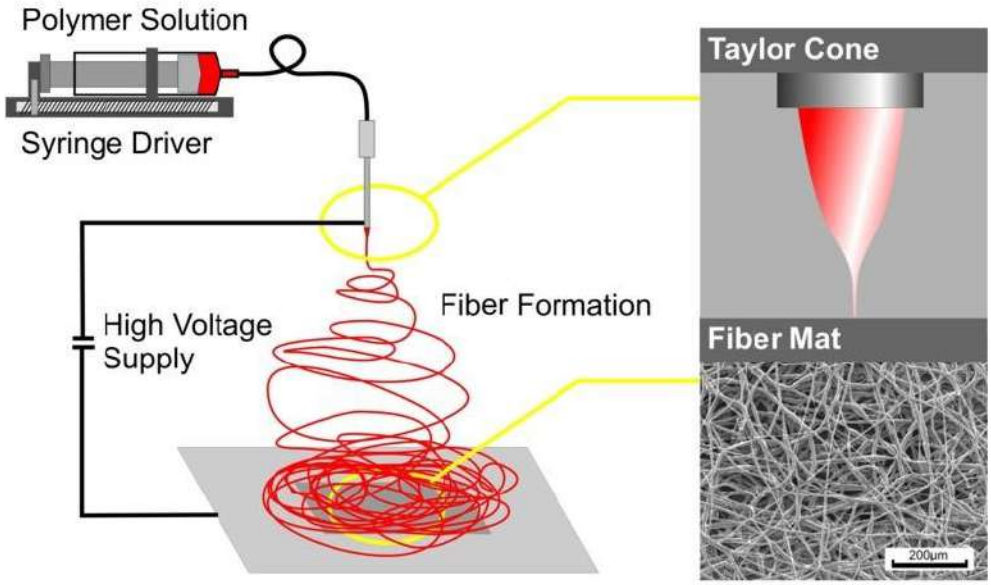

Fig. 1.12: Electrospinning technology for the fabrication of porous scaffolds.

CAD/CAM technologies

Because most of the above techniques are limited when it comes to the control of porosity and pore size, computer assisted design and manufacturing techniques have been introduced to tissue engineering. First, a three-dimensional structure is designed using CAD software. The porosity can be tailored using algorithms within the software [40]. The scaffold is then realized by using ink-jet printing of polymer powders or through Fused Deposition Modeling of a polymer melt.

A 2011 study by El-Ayoubi et al. investigated "3D-plotting technique to produce (biocompatible and biodegradable) poly-L-Lactide macroporous scaffolds with two different pore sizes" via solid free-form fabrication (SSF) with computer-aided-design (CAD), to explore therapeutic articular cartilage replacement as an "alternative to conventional tissue repair" [41].

The study found the smaller the pore size paired with mechanical stress in a bioreactor (to induce in vivo-like conditions), the higher the cell viability in potential therapeutic functionality via decreasing recovery time and increasing transplant effectiveness [42].

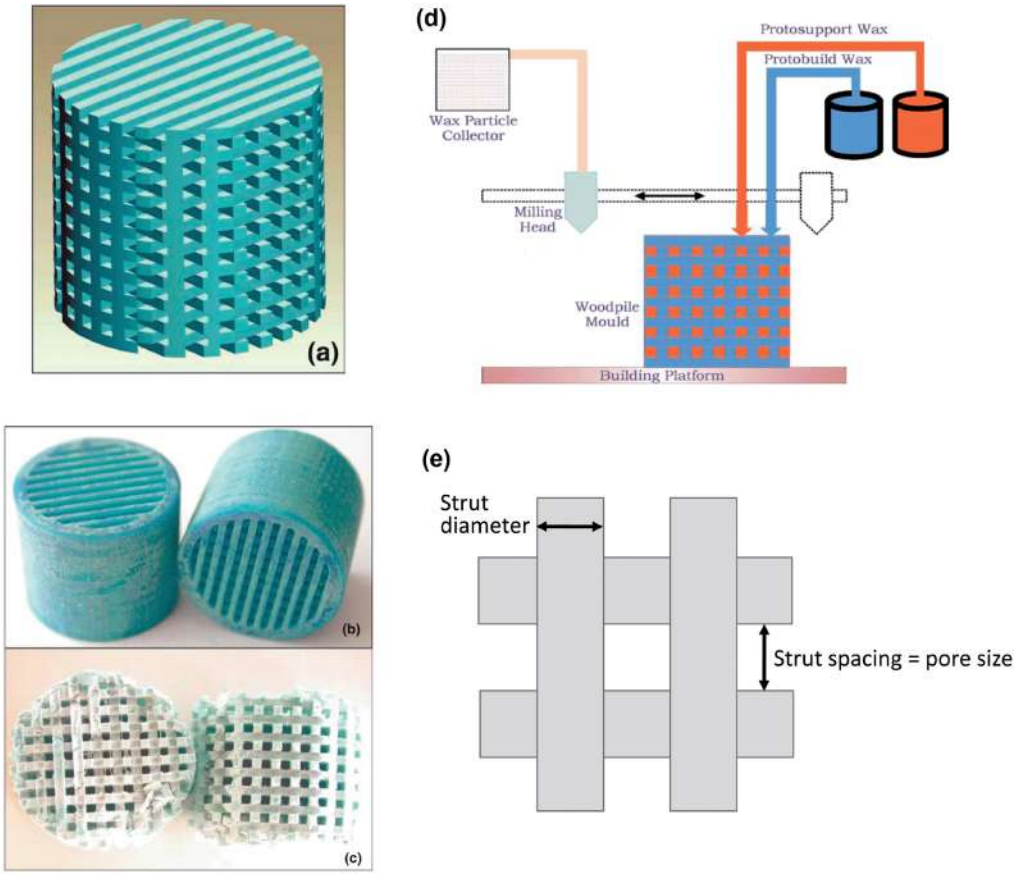

Fig. 1.13: CAD technology for the fabrication of 3D porous scaffolds with defined morphology.

Laser-assisted bioprinting

In a 2012 study, Koch et al. focused on whether Laser-assisted BioPrinting (LaBP) can be used to build multicellular 3D patterns in natural matrix, and whether the generated constructs are functioning and forming tissue. LaBP arranges small volumes of living cell suspensions in set high-resolution patterns. The investigation was successful, the researchers foresee that "generated tissue constructs might be used for in vivo testing by implanting them into animal models" [43]. As of this study, only human skin tissue has been synthesized, though researchers

project that "by integrating further cell types (e.g. melanocytes, Schwann cells, hair follicle cells) into the printed cell construct, the behavior of these cells in a 3D in vitro microenvironment similar to their natural one can be analyzed", useful for drug discovery and toxicology studies.

Assembly methods

One of the continuing, persistent problems with tissue engineering is mass transport limitations. Engineered tissues generally lack an initial blood supply, thus making it difficult for any implanted cells to obtain sufficient oxygen and nutrients to survive, or function properly.

Self-assembly

Self-assembly may play an important role here, both from the perspective of encapsulating cells and proteins, as well as creating scaffolds on the right physical scale for engineered tissue constructs and cellular ingrowth. The micromasonry is a prime technology to get cells grown in a lab to assemble into three-dimensional shapes. To break down tissue into single-cell building blocks, researchers have to dissolve the extracellular mortar that normally binds them together. But once that glue is removed, it's quite difficult to get cells to reassemble into the complex structures that make up our natural tissues. While cells aren't easily stackable, building blocks are. So the micromasonry starts with the encapsulation of living cells in polymer cubes. From there, the blocks self-assemble in any shape using templates.

Additive manufacturing

It might be possible to print organs, or possibly entire organisms using additive manufacturing techniques. A recent innovative method of construction uses an ink-jet mechanism to print precise layers of cells in a matrix of thermoreversible gel. Endothelial cells, the cells that line blood vessels, have been printed in a set of stacked rings. When incubated, these fused into a tube.

The field of three-dimensional and highly accurate models of biological systems is pioneered by multiple projects and technologies including a rapid method for creating tissues and even whole organs involves a 3D printer that can print the scaffolding and cells layer by layer into a working tissue sample or organ.

1.4.3. Bioreactors

A bioreactor in tissue engineering is a device that attempts to simulate a physiological environment in order to promote cell or tissue growth in vitro. A physiological environment can consist of many different parameters such as temperature and oxygen or carbon dioxide concentration, but can extend to all kinds of biological, chemical or mechanical stimuli. Therefore, there are systems that may include the application of forces or stresses to the tissue or even of electric current in two- or three-dimensional setups.

In academic and industry research facilities, it is typical for bioreactors to be developed to replicate the specific physiological environment of the tissue being grown (e.g., flex and fluid shearing for heart tissue growth). Several general-use and application-specific bioreactors are also commercially available, and may provide static chemical stimulation or combination of chemical and mechanical stimulation.

There are a variety of bioreactors designed for 3D cell cultures. There are small plastic cylindrical chambers, as well as glass chambers, with regulated internal humidity and moisture specifically engineered for the purpose of growing cells in three dimensions. The bioreactor uses bioactive synthetic materials such as polyethylene terephthalate membranes to surround the spheroid cells in an environment that maintains high levels of nutrients. They are easy to open and close, so that cell scaffolds can be removed for testing, yet the chamber is able to maintain 100% humidity throughout. This humidity is important to achieve maximum cell growth and function. The bioreactor chamber is part of a larger device that rotates to ensure equal cell growth in each direction across three dimensions.

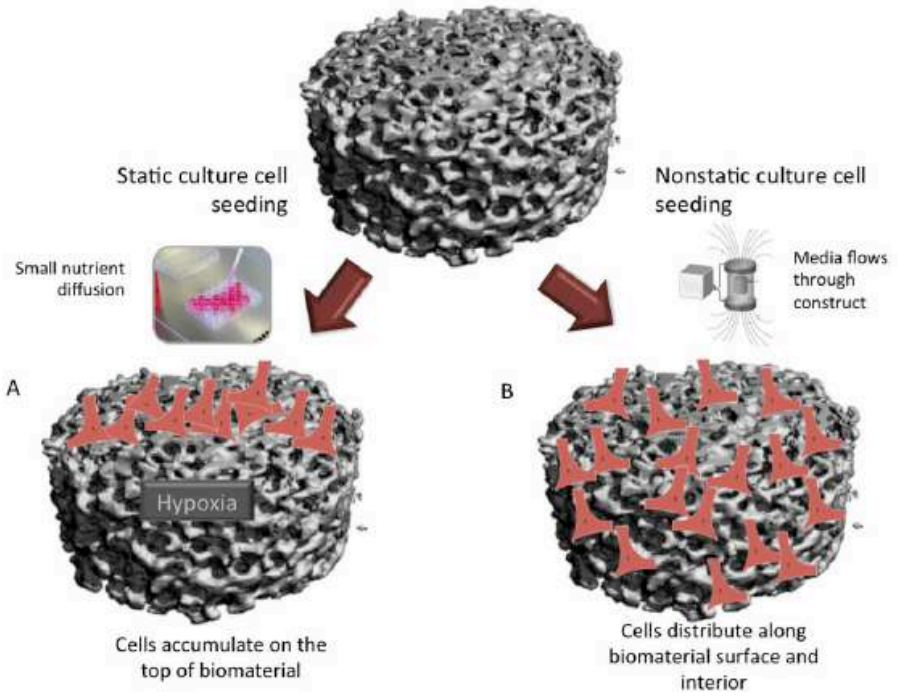

Fig. 1.14: Different interactions between cells and scaffolds if cultured in static or in dynamic (within bioreactor) conditions.

Main types of bioreactors are: spinner flask bioreactors, rotating wall bioreactors, compression bioreactors, flow perfusion bioreactors.

Spinner flask bioreactors

Spinner flask bioreactors are maybe the simplest and the most frequently used bioreactor types. Spinner bioreactor types mix the oxygen and nutrients throughout the medium and reduce the concentration boundary layer at the construct surface. In a spinner flask, scaffolds are suspended at the end of needles in a flask of culture media. A magnetic stirrer mixes the media and the scaffolds are fixed in place with respect to the moveing fluid. Flow across the surface of the scaffolds results in turbulences and flow instabilities caused by clumps of fluid particles that have a rotational structure superimposed on the mean linear motion of the fluid particles. Via these added fluid motions fluid transport to the centre of the scaffold is thought to be enhanced. Typically, spinner flasks are around 120 ml in

volume (although much larger flasks of up to 8 liters have also been used). The most frequent stirring speed is 50–80 rpm and generally 50% of the total medium is changed every two days. The efficiency of the enhancement of mass transport is indicated that cartilage constructs have been grown in spinner flasks to thicknesses of 0.5 mm compared to that of 100 mm in static cultures. However, cell seeding efficiency is typically low in spinner flask bioreactors, this method usually fails to deliver homogeneous cell distribution throughout scaffolds and cells predominantly reside on the construct periphery.

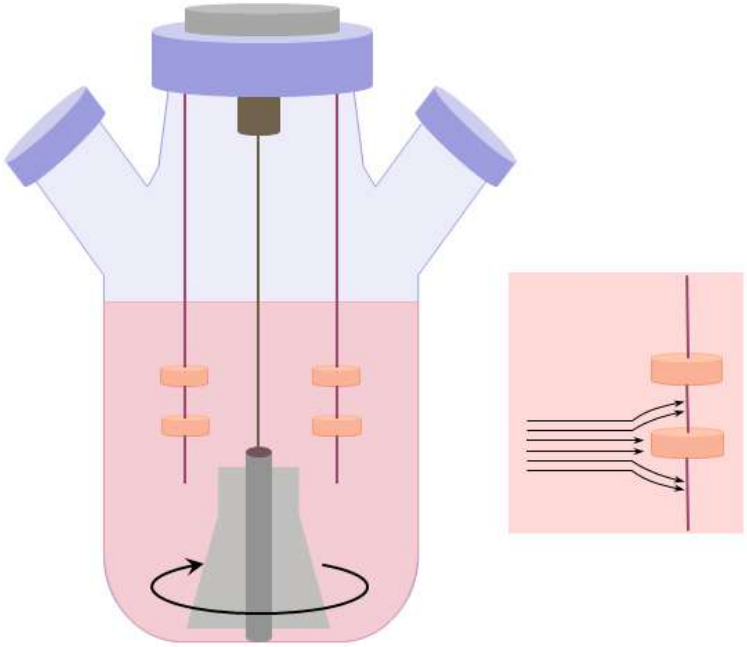

Fig. 1.15: Spinner flask bioreactor.

Rotating wall bioreactors

The rotating wall bioreactor was originally developed by NASA. It was designed with a view to protect cell culture experiments from high forces during space shuttle take off and landing. The device has proved useful in tissue engineering laboratories on Earth too. In a rotating wall bioreactor, scaffolds are free to move in media in a vessel. A rotating wall vessel bioreactor consists of a cylindrical chamber in which the outer wall, inner wall, or both are capable of rotating at a constant angular speed. The vessel

wall is then rotated at a speed such that a balance is reached between the downward gravitational force and the upward hydrodynamic drag force acting on each scaffold. The wall of the vessel rotates, providing an upward hydrodynamic drag force that balances with the downward gravitational force, resulting in the scaffold remaining suspended in the media. Dynamic laminar flow generated by a rotating fluid environment is an alternative and efficient way to reduce diffusional limitations of nutrients and wastes while producing low levels of shear compared to the stirring flask. Culture medium can be exchanged by stopping the rotation temporarily or by adding a fluid pump whereby media is constantly pumped through the vessel. Fluid transport is enhanced in a similar fashion to the mechanism in spinner flasks and the rotational devices also provide a more homogeneous cell distribution compared to static or spinner bioreactor cultures. Gas exchange occurs through a gas exchange membrane. Typically, the bioreactor is rotated at speeds of 15–30 rpm. Cartilage tissue of 5 mm thickness has been grown in this type of bioreactor after seven months of culture. As tissue mass increases while cells grow in the bioreactor, the rotational speed must be increased in order to balance the gravitational force and to ensure that the scaffold remains in suspension.

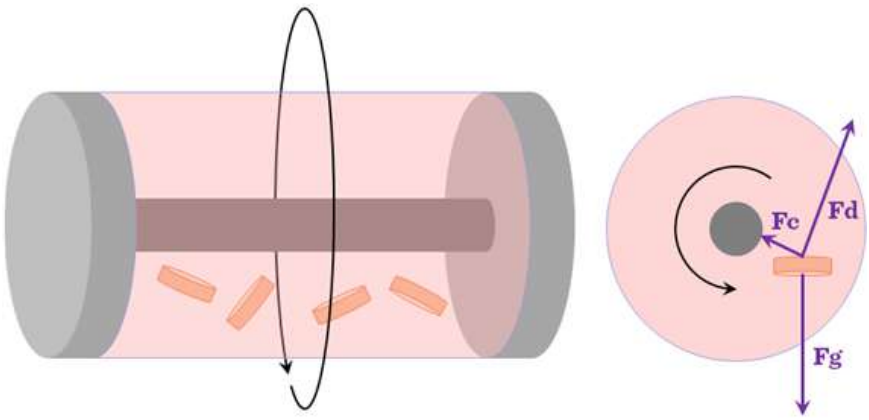

Fig. 1.16: Rotating wall bioreactor.

Compression bioreactors

Compression bioreactors are another widely used type of bioreactors. This class of bioreactor is generally used in cartilage engineering and can be designed so that both static and dynamic loading can be applied. In general, compression bioreactors consist of a motor, a system providing linear motion and a controlling mechanism to provide different magnitudes and frequencies. A signal generator can be used to control the system including loading of cells while transformers can be used to measure the load response and imposed displacement. The load can be transferred to the cell-seeded constructs via flat platens which distribute the load evenly. However, in a device for stimulating multiple scaffolds simultaneously, care must be taken that the constructs are of similar height or the compressive strain applied will vary as the scaffold height does. Mass transfer is improved in dynamic compression bioreactors over static culture (as compression causes fluid flow in the scaffold) which results in the improvement of the aggregate modulus of the resulting cartilage tissue to levels approaching those of native articular cartilage.

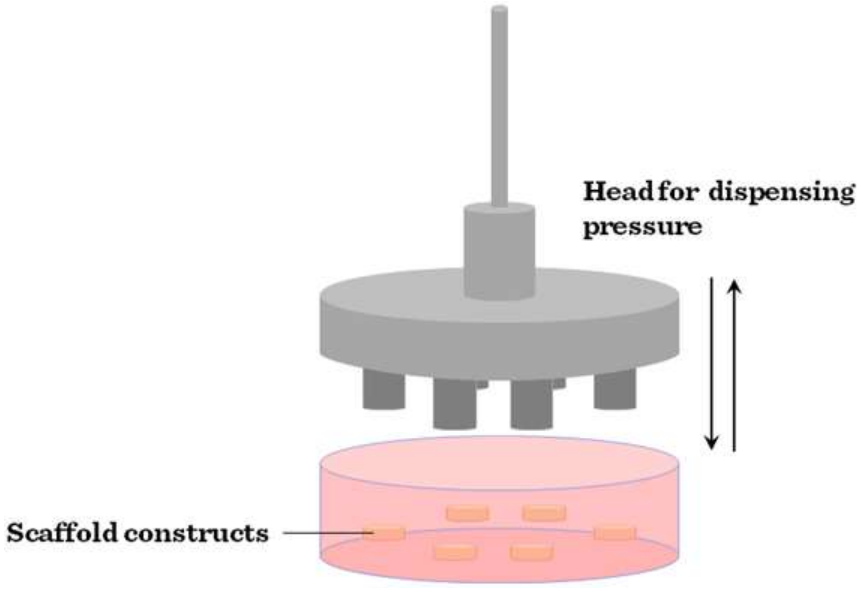

Fig. 1.17: Compressing bioreactor.

Perfusion bioreactors

Culture using flow perfusion bioreactors has been shown to provide more homogeneous cell distribution throughout scaffolds.

In comparisons between flow perfusion, spinner flask and rotating wall bioreactors, flow perfusion bioreactors have proved to be the best for fluid transport. Using the same flow rate and the same scaffold type, while cell densities remained the same using all three bioreactors, the distribution of the cells changed dramatically depending on which bioreactor was used. Histological analysis showed that spinner flask and static culture resulted in the majority of viable cells being on the periphery of the scaffold. In contrast, the rotating wall vessel and flow perfusion bioreactor culture resulted in uniform cell distribution throughout the scaffolds. Flow perfusion bioreactors generally consist of a pump and a scaffold chamber joined together by tubing. A fluid pump is used to force media flow through the cell-seeded scaffold. The scaffold is placed in a chamber that is designed to direct flow through the interior of the scaffold. The scaffold is kept in position across the flow path of the device and media is perfused through the scaffold, thus enhancing fluid transport. Media can easily be replaced in the media reservoir. However, the effects of direct perfusion can be highly dependent on the medium flow rate. Therefore optimising a perfusion bioreactor for the engineering of a 3D tissue must address the careful balance between the mass transfer of nutrients and waste products to and from cells, the retention of newly synthesised ECM components within the construct and the fluid induced shear stresses within the scaffold pores.

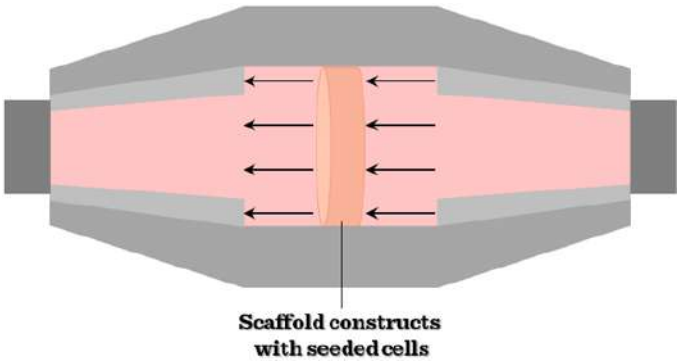

Fig. 1.18: Perfusion bioreactor.

1.5. Cancer Tissue Engineering

As previously seen, tissue engineering (TE) has evoked new hopes for the cure of organ failure and tissue loss by creating functional substitutes in the laboratory. Besides various innovations in the context of Regenerative Medicine (RM), TE also provides new technology platforms to study mechanisms of angiogenesis and tumour cell growth as well as potentially tumour cell spreading in cancer research. Such TE-Cancer research models allow us to investigate the interactions that occur when replicating physiological and pathological conditions during the initial phases of replication, morphogenesis, differentiation and growth under variable given conditions. Tissue microenvironment has been extensively studied in many areas of TE and it plays a crucial role in cell signalling and regulation of normal and malignant cell functions.

The synthesis of TE with innovative methods of molecular biology and stem-cell technology may help investigate and potentially modulate principal phenomena of tumour growth and spreading, as well as tumour-related angiogenesis.

The concept of cancer tissue engineering is very recent, but holds great promise. In 2006, at the dawn of cancer tissue engineering studies, the TE community pointed out their next generation guidelines, underlining the necessity of complex biomimetic models, nicely correlating stem cell differentiation on TE scaffolds with developmental biology. To achieve the formation of mature functional substitutes ex vivo, tissue engineers, were thus suggested to focus on the regeneration of metastable microenvironments, where complex cell-cell and cell-extracellular matrix (ECM) interactions can develop in a biomimetic fashion. Such guidelines actually also retrace the features that an optimal tumour modelling should have. In this view, cancer development biology can meet the TE approach with a renewed emphasis. These new platforms can be exploited to learn about fundamental cell-biomaterial interactions and cell-cell communications, being valid for both normal and cancer cells. When cell populations are used to form tissues and organs, proper 3D systems, with

clinically relevant dimensions, are required to eventually scale up these findings into effective new treatments.

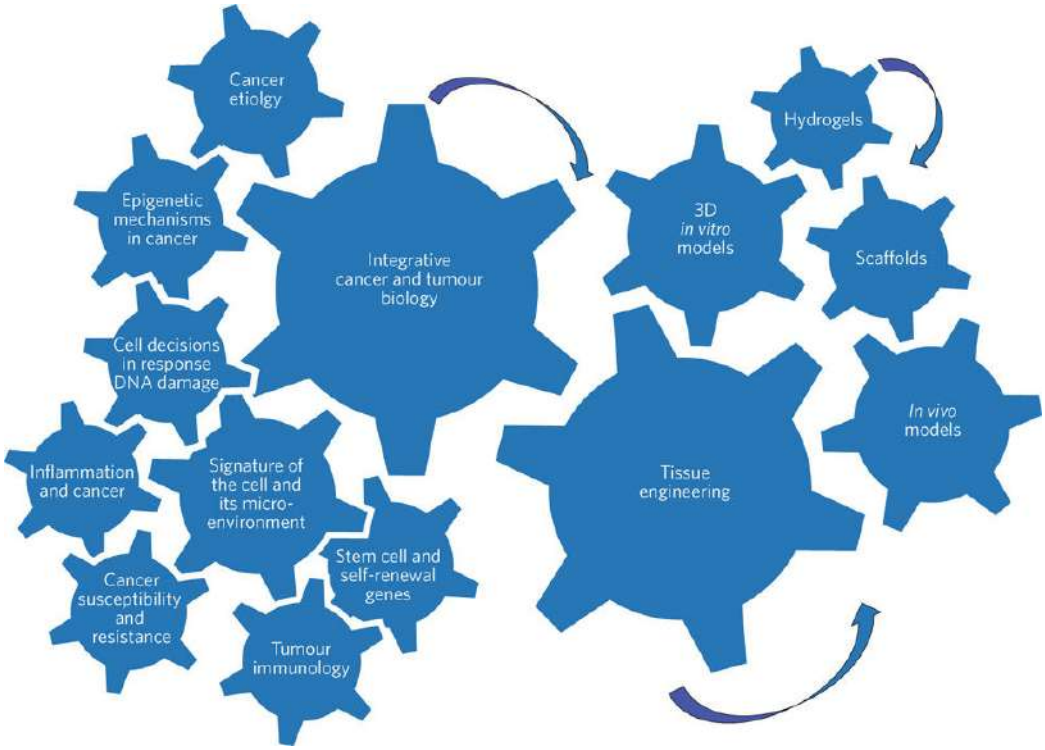

Figure 1.10. Integration of cancer biology and tissue engineering competences, at the base of the cancer tissue engineering concept.

1.6. References

1 Mukherjee, D. & Zhao, J. The Role of chemokine receptor CXCR4 in breast cancer metastasis. *Am J Cancer Res* **3**, 46-57 (2013).

2 Dawson, S.-J. *et al*. Analysis of circulating tumor DNA to monitor metastatic breast cancer. *New England Journal of Medicine* **368**, 1199-1209 (2013).

3 Scully, O. J., Bay, B.-H., Yip, G. & Yu, Y. Breast cancer metastasis. *Cancer Genomics-Proteomics* **9**, 311-320 (2012).

4 Slamon, D. J. *et al*. Use of chemotherapy plus a monoclonal antibody against HER2 for metastatic breast cancer that overexpresses HER2. *New England Journal of Medicine* **344**, 783-792 (2001).

5 Massagué, J. & Obenauf, A. C. Metastatic colonization by circulating tumour cells. *Nature* **529**, 298-306 (2016).

6 Paz, H., Pathak, N. & Yang, J. Invading one step at a time: the role of invadopodia in tumor metastasis. *Oncogene* **33**, 4193-4202 (2014).

7 Linder, S. The matrix corroded: podosomes and invadopodia in extracellular matrix degradation. *Trends in cell biology* **17**, 107-117 (2007).

8 Murphy, D. A. & Courtneidge, S. A. The'ins' and'outs' of podosomes and invadopodia: characteristics, formation and function. *Nature reviews Molecular cell biology* **12**, 413-426 (2011).

9 Yamada, K. M. & Cukierman, E. Modeling tissue morphogenesis and cancer in 3D. *Cell* **130**, 601-610 (2007).

10 Lovitt, C. J., Shelper, T. B. & Avery, V. M. Advanced cell culture techniques for cancer drug discovery. *Biology* **3**, 345-367 (2014).

11 Breslin, S. & O'Driscoll, L. Three-dimensional cell culture: the missing link in drug discovery. *Drug discovery today* **18**, 240-249 (2013).

12 Birgersdotter, A., Sandberg, R. & Ernberg, I. in *Seminars in cancer biology*. 405-412 (Elsevier).

13 Liu, H., Lin, J. & Roy, K. Effect of 3D scaffold and dynamic culture condition on the global gene expression profile of mouse embryonic stem cells. *Biomaterials* **27**, 5978-5989 (2006).

14 Zhang, S., Gelain, F. & Zhao, X. in *Seminars in cancer biology*. 413-420 (Elsevier).

15 Alberts, B. *et al*. Cell junctions, cell adhesion, and the extracellular matrix. (2002).

16 Hutter, J. L. & Bechhoefer, J. Calibration of atomic‐force microscope tips. *Review of Scientific Instruments* **64**, 1868-1873 (1993).

17 Peñuela, L. *et al*. Atomic force microscopy to investigate spatial patterns of response to interleukin-1beta in engineered cartilage tissue elasticity. *Journal of biomechanics* **47**, 2157-2164 (2014).

18 Oliver, W. C. & Pharr, G. M. An improved technique for determining hardness and elastic modulus using load and displacement sensing

indentation experiments. *Journal of materials research* **7**, 1564-1583 (1992).
19 Oliver, W. C. & Pharr, G. M. Measurement of hardness and elastic modulus by instrumented indentation: Advances in understanding and refinements to methodology. *Journal of materials research* **19**, 3-20 (2004).
20 Barenghi, R. *et al*. Elastin-coated biodegradable photopolymer scaffolds for tissue engineering applications. *BioMed research international* **2014** (2014).
21 Scaglione, S. *et al*. Order versus Disorder: in vivo bone formation within osteoconductive scaffolds. *Scientific reports* **2** (2012).
22 Scaglione, S. *et al*. In vivo lamellar bone formation in fibre coated MgCHA–PCL-composite scaffolds. *Journal of Materials Science: Materials in Medicine* **23**, 117-128 (2012).
23 Engler, A. *et al*. Substrate compliance versus ligand density in cell on gel responses. *Biophysical journal* **86**, 617-628 (2004).
24 Huang, X. *et al*. Matrix Stiffness in Three‐Dimensional Systems Effects on the Behavior of C3A Cells. *Artificial organs* **37**, 166-174 (2013).
25 Markert, C. D. *et al*. Characterizing the micro-scale elastic modulus of hydrogels for use in regenerative medicine. *journal of the mechanical behavior of biomedical materials* **27**, 115-127 (2013).
26 Agarwal, A. *et al*. Micropatterning alginate substrates for in vitro cardiovascular muscle on a chip. *Advanced functional materials* **23**, 3738-3746 (2013).
27 Cukierman, E., Pankov, R., Stevens, D. R. & Yamada, K. M. Taking cell-matrix adhesions to the third dimension. *Science* **294**, 1708-1712 (2001).
28 Tibbitt, M. W. & Anseth, K. S. Hydrogels as extracellular matrix mimics for 3D cell culture. *Biotechnology and bioengineering* **103**, 655-663 (2009).
29 Kenny, P. A. *et al*. The morphologies of breast cancer cell lines in three-dimensional assays correlate with their profiles of gene expression. *Molecular oncology* **1**, 84-96 (2007).
30 Cavo, M. *et al*. Microenvironment complexity and matrix stiffness regulate breast cancer cell activity in a 3D in vitro model. *Scientific reports* **6** (2016).
31 Amaro, A. *et al*. A highly invasive subpopulation of MDA-MB-231 breast cancer cells shows accelerated growth, differential chemoresistance, features of apocrine tumors and reduced tumorigenicity in vivo. *Oncotarget* **7**, 68803 (2016).
32 Mathew, B. *et al*. Robust and automated three-dimensional segmentation of densely packed cell nuclei in different biological specimens with Lines-of-Sight decomposition. *BMC bioinformatics* **16**, 187 (2015).
33 Deitzel, J. M., Kleinmeyer, J., Harris, D. E. A. & Tan, N. C. B. The effect of processing variables on the morphology of electrospun nanofibers and textiles. *Polymer* **42**, 261-272 (2001).

34 Khil, M. S., Cha, D. I., Kim, H. Y., Kim, I. S. & Bhattarai, N. Electrospun nanofibrous polyurethane membrane as wound dressing. *Journal of Biomedical Materials Research Part B: Applied Biomaterials* **67**, 675-679 (2003).

35 Hotary, K., Li, X.-Y., Allen, E., Stevens, S. L. & Weiss, S. J. A cancer cell metalloprotease triad regulates the basement membrane transmigration program. *Genes & development* **20**, 2673-2686 (2006).

36 Lee, G. Y., Kenny, P. A., Lee, E. H. & Bissell, M. J. Three-dimensional culture models of normal and malignant breast epithelial cells. *Nature methods* **4**, 359 (2007).

37 Kim, M. S. *et al*. Highly porous 3D nanofibrous scaffolds processed with an electrospinning/laser process. *Current Applied Physics* **14**, 1-7 (2014).

38 Beachley, V. & Wen, X. Effect of electrospinning parameters on the nanofiber diameter and length. *Materials Science and Engineering: C* **29**, 663-668 (2009).

39 Doerr, M. E. & Jones, J. I. The roles of integrins and extracellular matrix proteins in the insulin-like growth factor I-stimulated chemotaxis of human breast cancer cells. *Journal of Biological Chemistry* **271**, 2443-2447 (1996).

40 Del Monte, U. Does the cell number 109 still really fit one gram of tumor tissue? *Cell Cycle* **8**, 505-506 (2009).

41 Krebs, M. G., Hou, J.-M., Ward, T. H., Blackhall, F. H. & Dive, C. Circulating tumour cells: their utility in cancer management and predicting outcomes. *Therapeutic advances in medical oncology* **2**, 351-365 (2010).

42 Albini, A. & Benelli, R. The chemoinvasion assay: a method to assess tumor and endothelial cell invasion and its modulation. *Nature protocols* **2**, 504-511 (2007).

43 Bharadwaj, S., Thanawala, R., Bon, G., Falcioni, R. & Prasad, G. L. Resensitization of breast cancer cells to anoikis by tropomyosin-1: role of Rho kinase-dependent cytoskeleton and adhesion. *Oncogene* **24**, 8291 (2005).

Chapter 2

Thesis objectives

The aim of this thesis is the study, development and validation of new in vitro 3D tumor models through the use of bioengineering and tissue engineering approaches. Among all solid tumours, we focused our attention on breast cancer, the most common cancer in women.

- The study on a new model of low aggressive breast cancer has the aim to provide a realistic model of 3D primary breast tumour. In this work, I used mechanically tuned alginate hydrogels to study the role of substrate elasticity on breast adenocarcinoma cell activity. I observed a strict correlation between cell viability and substrate elasticity; in particular, the highest cellular proliferation rate, associated with the formation of typical cell clusters, occurred in two weeks only in the softest hydrogels (E = 150–200 kPa).

- Considering the importance of breast cancer metastasis, the study on a new model of highly aggressive breast cancer has the aim to provide a 3D in vitro model able to allow cells to show some key features related to their motility and aggressive potential. To this aim, we developed composite gels constituted by different concentrations of Alginate (A) and Matrigel (M) to obtain a structurally stable-in-time and biologically active substrate. Human aggressive breast cancer cells (i.e. MDA-MB-231) were cultured within the gels. A particular type of gel (i.e. 50% Alginate, 50% Matrigel) emerged thanks to a series of significant results: cells exhibited peculiar cytoskeleton shapes and

poly-nuclei organization characteristic of their malignancy; cells expressed the formation of the so-called invadopodia, actin-based protrusion of the plasma membrane through which cells anchor to the extracellular matrix; cells were able to migrate through the gels and attach to an engineered membrane mimicking the vascular walls hosted within bioreactor.

- Finally, a full set-up was developed to observe in vitro cell detachment from a primary tumor model and entering in circulation. We combined a bioreactor-based bioengineering approach with single cell analysis of Circulating Tumor Cells (CTCs). Analysis of human CTCs has now revealed important features of cancer metastasis, such as the high metastatic potential of CTC-clusters compared to single CTCs. For this reason, we applied the same approach to our in vitro system. Single cell qPCR of the circulating LM2 cells was performed. A proof-of-concept that the approach can work was performed, as well as evidence that the cells can be extracted from the device and used for molecular analysis.

Chapter 3

3D in vitro model of low aggressive breast cancer

3.1. Abstract

Three-dimensional (3D) cell cultures represent fundamental tools for the comprehension of cellular phenomena both in normal and in pathological conditions. In particular, mechanical and chemical stimuli play a relevant role on cell fate, cancer onset and malignant evolution. In this work, I used mechanically-tuned alginate hydrogels to study the role of substrate elasticity on breast adenocarcinoma cell activity. The hydrogel elastic modulus (E) was measured via atomic force microscopy (AFM) and a remarkable range (150–4000 kPa) was obtained. A breast cancer cell line, MCF-7, was seeded within the 3D gels, on standard Petri and alginate-coated dishes (2D controls). Cells showed dramatic morphological differences when cultured in 3D versus 2D, exhibiting a flat shape in both 2D conditions, while maintaining a circular, spheroid-organized (cluster) conformation within the gels, similar to those in vivo. Moreover, we observed a strict correlation between cell viability and substrate elasticity; in particular, the number of MCF-7 cells decreased constantly with increasing hydrogel elasticity. Remarkably, the highest cellular proliferation rate, associated with the formation of cell clusters, occurred at two weeks only in the softest hydrogels (E = 150–200 kPa), highlighting the need to adopt more realistic and a priori defined models for in vitro cancer studies.

3.2 Materials and methods

3.2.1. 3D alginate gel preparation

Three-dimensional alginate gels were prepared as follows. Firstly, 1% (w/v) agar solutions containing calcium ions (solutions A) were prepared by mixing Agar (DIFCO Laboratories) in physiological buffer enriched with different concentrations (0.2 M, 0.5 M or 1 M) of CaCl2 (J. T. Baker). The solutions were brought to the boil, poured into 6-well plates until 1 cm height was obtained and allowed to cool until complete solidification. Holes of 0.5 cm diameter were then cut in the agar, using a Pasteur glass pipette, to make gel molds. Alginate solutions, 0.5% (w/v), 1% (w/v) or 2% (w/v), were prepared by mixing Alginate (Manugel GMB, FMC BioPolymer) in physiological buffer (solutions B). Effective intimate mixing of the alginate solutions was carried out for 12 h at room temperature under vigorous magnetic stirring. The solutions were then stored at 4 °C. Next, 120 µl of each solution B was dispensed into the selected gel molds using a syringe. Gelation was allowed to take place at 37 °C for 1 hour, in order to ensure complete diffusion of calcium ions from the agar to the alginate solution. The alginate hydrogels were then extracted from the gel molds and maintained in a buffer containing 5 mM CaCl2.

3.2.2 Atomic Force Microscopy (AFM) nanoindention

Atomic force microscopy (AFM) was used to measure gel stiffness. To do this, we used a commercial AFM microscope (Keysight Technologies 5500 ILM) equipped with a closed loop scanner capable of 9µm vertical range. The scanner was always operated in “closed loop” in order to compensate for piezo nonlinearity, creep and hysteresis. A rectangular, 250 µm long, silicon microcantilever with sharp conical tips and a cone angle of 22° was used (CSG 11 type, NT-MDT, Russia). The cantilever spring constant was calculated by monitoring the cantilever oscillation in air due

to thermal noise, following the procedure described by Hutter and Bechhoefer [1].

Gels were glued onto a Petri dish using a minimum amount of fast cyanoacrylate glue. During the gluing step, the specimens stayed less than a minute out of the solution [2]. During measurement, samples were kept in a buffer containing 5 mM $CaCl_2$.

AFM indentation measurements were performed by recording a standard force curve and then calculating the corresponding load versus indentation curve.

The applied load for any given cantilever deflection was calculated by first converting the output voltage, from the AFM four-segment photodetector, into nanometers of deflection (sometime referred to as "inverse optical lever sensitivity"), and then by multiplying the deflection by the cantilever spring constant. The conversion factor was calculated by taking several force curves on a hard glass substrate, every time the laser spot on the cantilever had to be adjusted, and considering the reciprocal of the average slope of the constant compliance region of the curves.

In order to take into account intra-sample heterogeneity, $16 \times 16 = 256$ force curves were recorded over a regular grid over a 5×5 mm^2 area. Each force curve was taken at a constant vertical displacement speed of 6 mm/s and with a maximum applied load that varied from sample to sample in order to get a maximum sample deformation (i.e. indentation) of 100 nm. Single force curves were processed in a semi-automatic way using a custom built software in order to i) detect the vertical displacement corresponding to the AFM probe-gel surface contact (during this procedure 10% of the curves on average were discarded due to noise or artefacts during acquisition which prevented the detection of the point of contact), ii) extract the applied load P as a function of the sample indentation h (the so-called load-indentation curve).

In order to calculate the Young's modulus of the gel we considered the unloading portion of the load-indentation curve to avoid effects due to plastic deformations and referred to the model for a quasi-static indentation

with a conical indenter originally proposed by Oliver and Pharr [3] and then refined by the same authors [4]:

$$E = 221 - \nu 2SA$$

where: ν is the Poisson's ratio of the hydrogel

A is the projected indenter contact area at a given indentation

S the contact stiffness, defined as the derivative of the load-indentation curve at the same indentation.

We calculated, for all measurements, contact area and stiffness at the maximum indentation $h_{max} = 100$ nm. Applying the same model, in order to calculate the derivative at h_{max}, we fitted the load-indentation relation with a power law: $P = a \cdot hm$ where a and m are the fitting parameters (m lays in the range 1.5-2 for a conical indenter [4]).

We assumed, for the Poisson's ratio of all tested gels, a constant value of $\nu = 0.5$, corresponding to an uncompressible, rubber like, material.

On a single gel sample, at least three maps of 16×16 curves over grouped collected onto macroscopically different positions randomly selected over the sample surface. Hence the reported elasticity value for each gel type corresponds to the average of at least 690 single measurements and evaluations of the Young's modulus.

Statistical evaluation was performed using the non-parametric Mann-Whitney test to determine significant differences among groups. The significance level was set at $p<0.05$. All results are presented as mean ± standard deviation.

It should be noted that the indentation measurements were not performed in quasi-static conditions and therefore the viscous response (loss modulus) might play a significant role; moreover the calculated absolute values of elasticity are prone to several uncertainties and non-idealities (e.g. in the tip geometry or the gel Poisson's ratio). Nevertheless, since all AFM measurements reported in this paper were taken with the same cantilever

and the same experimental conditions, the observed relative changes in stiffness are not significantly affected by the above uncertainties.

3.2.3 MCF-7 cell culture

The MCF-7 (breast adenocarcinoma) cell line was obtained from Sigma Aldrich. Cells were expanded in Eagle's minimal essential medium (EMEM) enriched with 10% Fetal Bovine Serum (FBS), 1% L-glutamine and 1% penicillin/streptomycin (all from Sigma Aldrich). When the required confluence was reached, cells were detached with 1X trypsin and counted. Cell seeding within the gels was achieved by directly suspending cells in sterile alginate solution in order to obtain an inoculum of 105 cells/sample. Culture medium enriched with 5 mM CaCl2 was then added. Two-dimensional cell cultures were carried out as a control to evaluate whether differences occurred on cells when cultured in 2D or 3D conditions. To this aim, MCF-7 cells were seeded at 3500 cells/cm2 density on both standard plastic and alginate-coated Petri dishes.

Both 2D and 3D cell cultures were incubated for up to 2 weeks at 37° C in an atmosphere of 5% CO2 to allow gas exchange. Medium was changed twice a week. At least duplicate samples were used for each assessment.

3.2.4 Live/Dead staining

After 7 days, cellular viability was analyzed in the 3D gels. For this purpose, gels were washed with phosphate-buffered saline (PBS) and incubated with a Live/Dead stain (Live/Dead Cell Double Staining Kit, Sigma Aldrich) at 37° C for 15 minutes.

Gels were then imaged by using an upright microscope equipped with transmitted illumination and epifluorescence (Eclipse Ni-U, Nikon)[20] to discriminate live cells (calcein AM stained-green) from dead cells (propidium iodide stained-red).

3.2.5 Flow cytometry

After 1 week, at least three gels per type were de-cross-linked by incubating them for 2 hours with a 1:1 (v/v) solution of 50 mM EDTA and complete medium. Cells were suspended in PBS enriched with 2% FBS (v/v) and stained for 5 minutes by incubating in Propidium Iodide (PI) solution (1% v/v). Flow cytometry was performed on a FACS Calibur system to obtain total and dead cell (PI-stained) counts.

3.2.6. Confocal fluorescence microscopy and morphological analysis

To examine the spatial distribution and morphology of cells, both 2D and 3D samples were analysed by optical confocal laser-scanning microscopy. For all typologies, samples were fixed, after 1 week, with 4% paraformaldehyde and treated with 0.1% Triton X-100 to permeabilize the cell membrane. Nuclei were stained with 1 μg/ml 4,6-Diamidino-2-phenylindole (DAPI), while actin filaments were stained with 100 μM Alexa Fluor 488 Phalloidin (all Sigma-Aldrich). Images were acquired by a confocal laser-scanning microscope (Leica TCS SP5 AOBS). Alexa Fluor 488 was excited with the 488 nm line of the Ar laser and its fluorescence was collected in a spectral window of 500 to 530 nm. For DAPI, 720 nm excitation wavelength and 450-500 nm spectral window emission were used.

Images were then analysed by ImageJ to measure and quantify several morphological features characterizing cells grown both in 3D and in 2D conditions. In particular, the following parameters were considered: Area of the cell; Perimeter of the cell; Major Axis and Minor Axis of the best fitting ellipse; Circularity, defined as 4πArea/Perimeter^2; Roundness, defined as Minor Axis/Major Axis.

3.2.7 Histology and cluster analysis

After 1 and 2 weeks of culture, the 3D alginate hydrogels were processed for histological analysis in order to observe the time-dependent

evolution of cell clusters. Briefly, samples were fixed in 4% buffered formalin for 3 hours and dehydrated in ethanol scale for a total of 6 hours. The samples were then paraffin embedded, cross-sectioned (7-μm thick) at different levels and stained with haematoxylin–eosin (H&E)[21,22]. Images were acquired by using a Nikon H550L optical microscope.

We evaluated two parameters of cell clusters: dimension and density.

For dimension analysis, at least 10 clusters (intended as group of communicating cells) were considered for each hydrogel, and the major axis of each cluster (i.e. cluster size) was measured. These values were subdivided into ranges (i.e. <10 mm, 10-30 mm, 30-50 mm, 100-150 mm, 150-200 mm, 200-250 mm, >250 mm) and clusters classified; results are presented as percentage of occurrence (Figure 6).

Cluster density, defined as:

$$D = \sum \text{cells area within a} \frac{\text{cluster}}{\text{cluster}} \text{area (\%)}$$

was quantified. To this aim, images of clusters were post-processed by using Image J platform: they were converted to 8-bit images and an automatic threshold was applied to discriminate the space occupied by cells (black) from the background (white). Threshold accuracy was checked manually for each image. Cluster density was calculated, in percentage, as ratio between black space and the total area of the cluster.

3.3. Results

3.3.1. 3D alginate gel realization

The adopted protocol produced 3D alginate gels, chemically cross-linked via radial diffusion of calcium ions (Figure 1, panels A, B). Structural differences among gels produced with different cross-linker

molarities and alginate concentrations were clearly observable: in detail, gels with 2% alginate solution and cross-linked with 0,5 M CaCl2 appeared structurally more compact and three-dimensionally defined than gels produced with either a lower concentration of alginate or a lower CaCl2 molarity (data not shown). In accordance with the dimensions of the gel molds, we obtained circular alginate gels, with ~5 mm diameter and ~3 mm height (Figure 1, panel C).

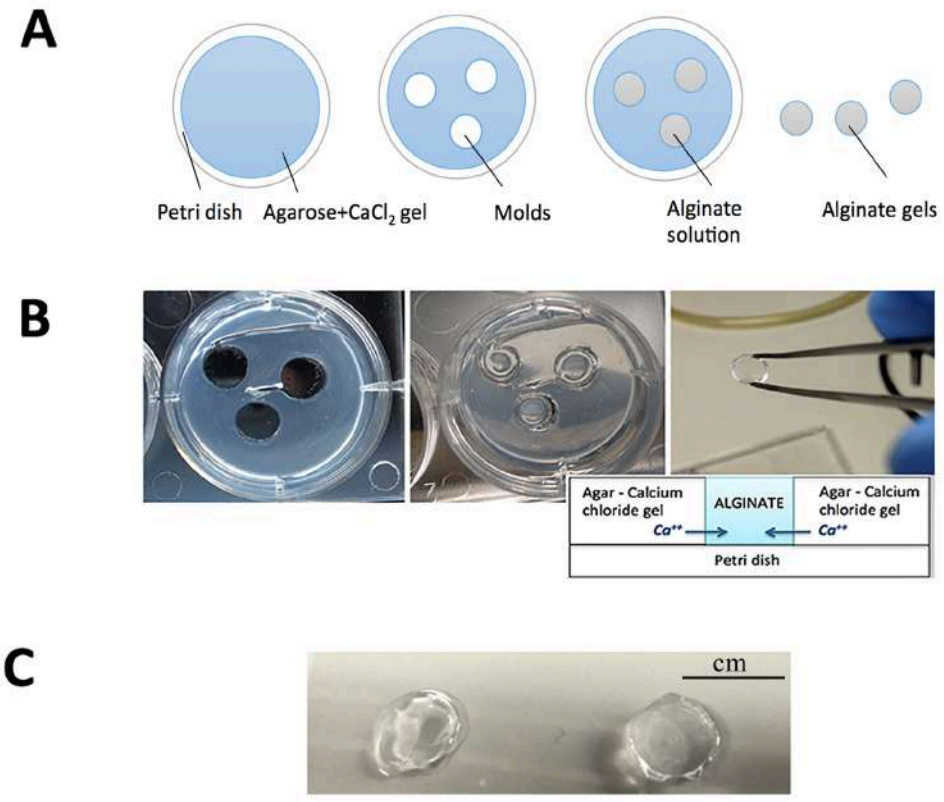

Figure 3.1: Gel manufacturing process. The protocol adopted for realization of the alginate gel consists of several steps, as summarized in the following picture: realization of the agar gel enriched with Calcium ions; realization of the gel molds, in the agar plates, using a Pasteur glass pipette; introduction of the alginate solution into the gel molds and alginate gelation. Panel A is a cartoon of these steps, while panel B shows some pictures of the experimental realization. Panel C shows two types of alginate gel samples prepared with 0.5% w/v (left) and 2% w/v (right) alginate solution and cross-linked with 0.5 M CaCl2 (scale bar: cm).

3.3.2. Gel mechanical characterization by AFM

The elastic modulus of each gel was measured at the sub-micrometer scale, the same length scale of the actual cell sensing[23], using AFM nanoindentation technique.

Figure 2 (panels A-B) shows, as an example, three representative indentation measurements for gels with 1 M CaCl2 and different alginate concentrations. The average force map (256 curves taken on a 5x5 μm^2 area) of both the raw force-distance curves (panel A) and the corresponding load-indentation curves (panel B) are displayed. The latter were used to calculate the Young's modulus of the gel. The curves show a qualitative, yet evident, difference in the compliance of the different gels while deformed by the AFM tip. Figure 2, panel C, reports the mean values and their dispersion of the Young's modulus measured over the gel surface by AFM nanoindentation, following the procedure described in the methods section. As evidenced, a weaker cross-linker content (i.e. 0.2 M CaCl2) did not allow significantly different stiffnesses to be obtained among the gels, despite the increase in alginate percentage. On the contrary, the elastic moduli were significantly different at 0.5-1-2% alginate concentrations when gels were cross-linked with higher CaCl2 content (i.e. 0.5 M and 1 M). Gels with overlapping ranges of stiffness (i.e. 0.5% alginate-0.5 M CaCl2 with 0.5% alginate-1 M CaCl2 and 2% alginate-0.5 M CaCl2 with 1% alginate-1 M CaCl2) were merged as a unique range, to finally obtain four different categories of stiffness in which the gels were subdivided (i.e. 150-200 kPa; 300-350 kPa; 900-1800 kPa; 2500-4000 kPa).

Our results demonstrate that gel stiffness is highly dependent on CaCl2 cross-linker concentration. Table 1 reports some values from the literature[24-26] on alginate gel elastic modulus, measured by AFM nanoindentation. Although CaCl2 concentrations do not overlap with our samples, the trend of increasing stiffness with an increase in both alginate and CaCl2 concentrations is in agreement with our observations.

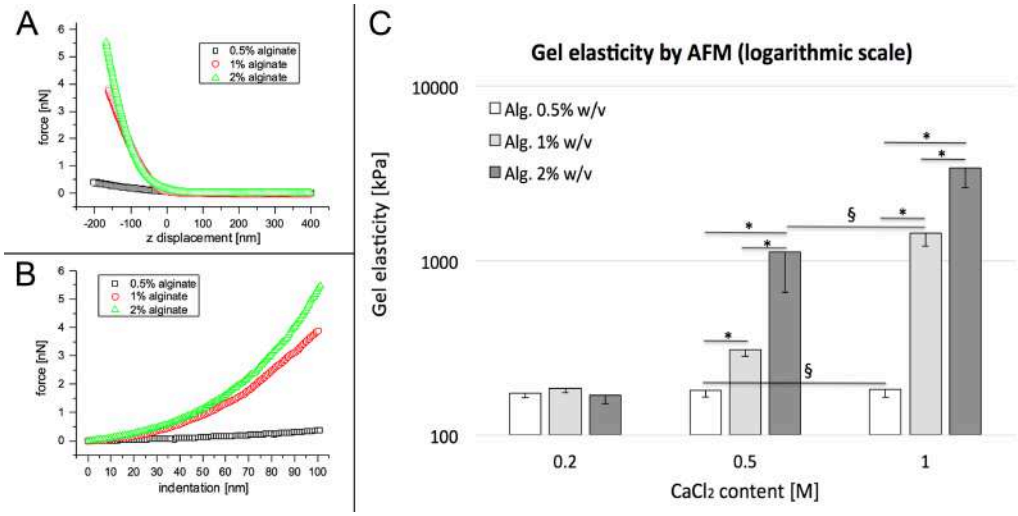

Figure 3.2: Gel mechanical characterization. Gel stiffness was measured by Atomic Force Microscopy. Panel A shows three representative force versus vertical displacement curves (average of 256 curves, full approachretraction cycle is plotted) measured on three different gels (0.5% w/v, 1% w/v and 2% w/v alginate, all crosslinked with 1 M CaCl2). The z = 0 corresponds to the vertical piezo displacement where the AFM tip gets into contact with the gel surface. Panel B shows the plots of the corresponding load versus indentation curves; only the unloading portions are plotted. Panel C shows the elastic modulus (average and standard deviation, STD) for the different gels probed by AFM nanoindentation: bar colours correspond to different alginate concentrations, while calcium molarity is shown along the x axis. Symbol *indicates samples with statistically different elasticity (Mann-Whitney test, $p < 0.05$). Symbol Åòindicates gels with elasticity ranges that are overlapped.

3.3.3. Cell viability

Cell viability in the alginate gels was evaluated after 7 days of culture using both the Live/Dead cell assay and FACS analysis. In detail, we used a fluorescence-based Live/Dead assay to acquire qualitative information on cell vitality, while FACS analysis was used to obtain a semi-quantitative outcome on cell number within each gel type. From the images in Figure 3, panel A, it is observable that only a few dead cells were found in gels after 7 days, confirming alginate as a promising substrate for cell culture and

validating the adopted gelation protocol. However, a deep discrepancy in cell colonization among different gel types was evident.

For FACS analysis, MCF-7s were firstly characterized (Figure 3, panels B and C) to set the best operational conditions; the number of live and dead cells was then derived for each gel type in relation to substrate stiffness (Figure D). FACS analysis confirmed and highlighted the differences in cell viability of the various gel types; in particular, the detected amount of cells is higher in gels characterized by a lower elastic modulus. The number of live cells seems to be influenced by substrate stiffness, while the number of dead cells (determined by propidium Iodide staining) is independent of substrate stiffness.

3.3.4. Cell morphology: 2D versus 3D

Cell morphology and organization in 3D gels were analysed by observing cytoskeleton orientation and cell-to-cell contact using a confocal microscope. As the control, MCF-7 cells, seeded on both standard and alginate-coated Petri dishes, were observed.

As expected[27,28], the morphological observation after one week of culture showed alarming morphological differences between cells in 2D and 3D. In particular, cells showed a flat morphology and were organized in a monolayer when seeded in standard or alginate-coated Petri dishes (Figure 4, panels A and B). In contrast, cells embedded within 3D gels were characterized by a round shape and cluster organization (Figure 4, panel C). Several cell colonies were observed, and multiple nuclei were present in each colony meaning that each cluster consisted of many cells. These differences are of great impact considering that changes in morphology often go hand-in-hand with biochemical changes, as demonstrated by other scientists: in 2007, Kenny et al. not only showed that strong differences occurred in breast cancer cells when cultured in 2D or 3D, but classified several breast cancer cell lines with different aggressiveness, as proven by gene expression analysis, into four distinct morphological groups: Round, Mass, Grape-like and Stellate. In that study, MCF-7 cells belonged to the

Mass group, since they formed colonies with disorganized nuclei and filled colony centres[29].

Going beyond the current state-of-the-art, we measured the changes in MCF-7 morphological features when cultured in different dimensional configurations (2D or 3D). Our results show that cells in 3D are characterized by a greater Area and Perimeter than in 2D, and by a greater balance between Major and Minor Axes. Consequently, they show higher values of Roundness than cells in 2D, characterized by elongated shapes. Circularity values are not statistically different among the different conditions (Figure 4, panel D).

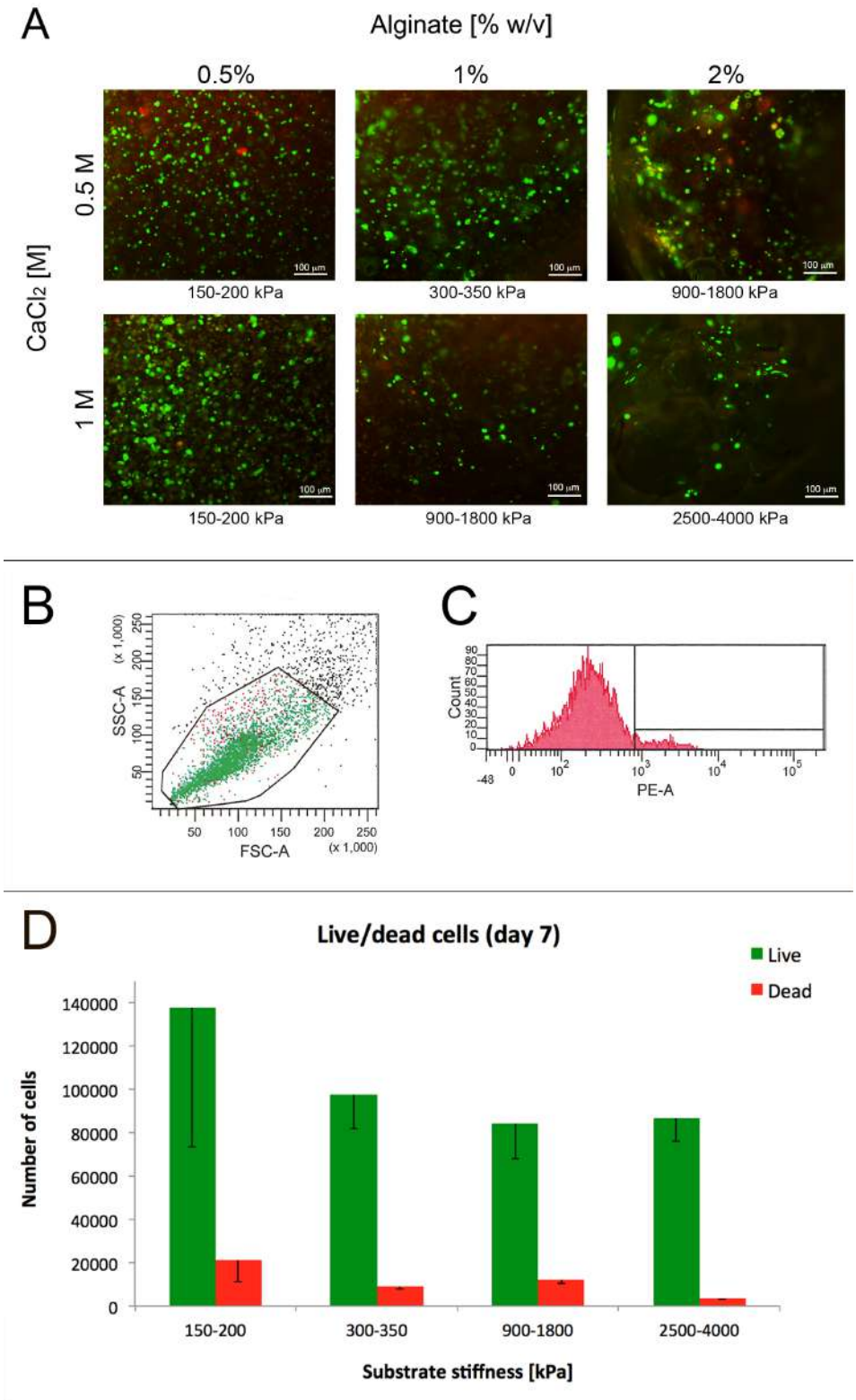

Figure 3.3: Cell viability. Representative images of live (green) and dead (red) MCF-7 cells encapsulated in alginate hydrogels with different alginate and CaCl2 concentrations, after 7 days of culture; images were acquired by fluorescence microscopy after treating samples with a Live/Dead assay;

gels are co-labelled with their stiffness (panel A). Flow cytometric analysis of MCF-7 cells after 7 days of 3D culture in alginate gels. Viability of cells was analysed by setting a gate based on the Side- (SSC) and Forward- (FSC) light SCatter (panel B), and measuring the percentage of PI positive staining cells within the gate, indicating dead cells (panel C). Number of live and dead cells per sample type (samples with different stiffness), after 7 days, estimated by FACS analysis (panel D). Error bar represents Standard Deviation (STD).

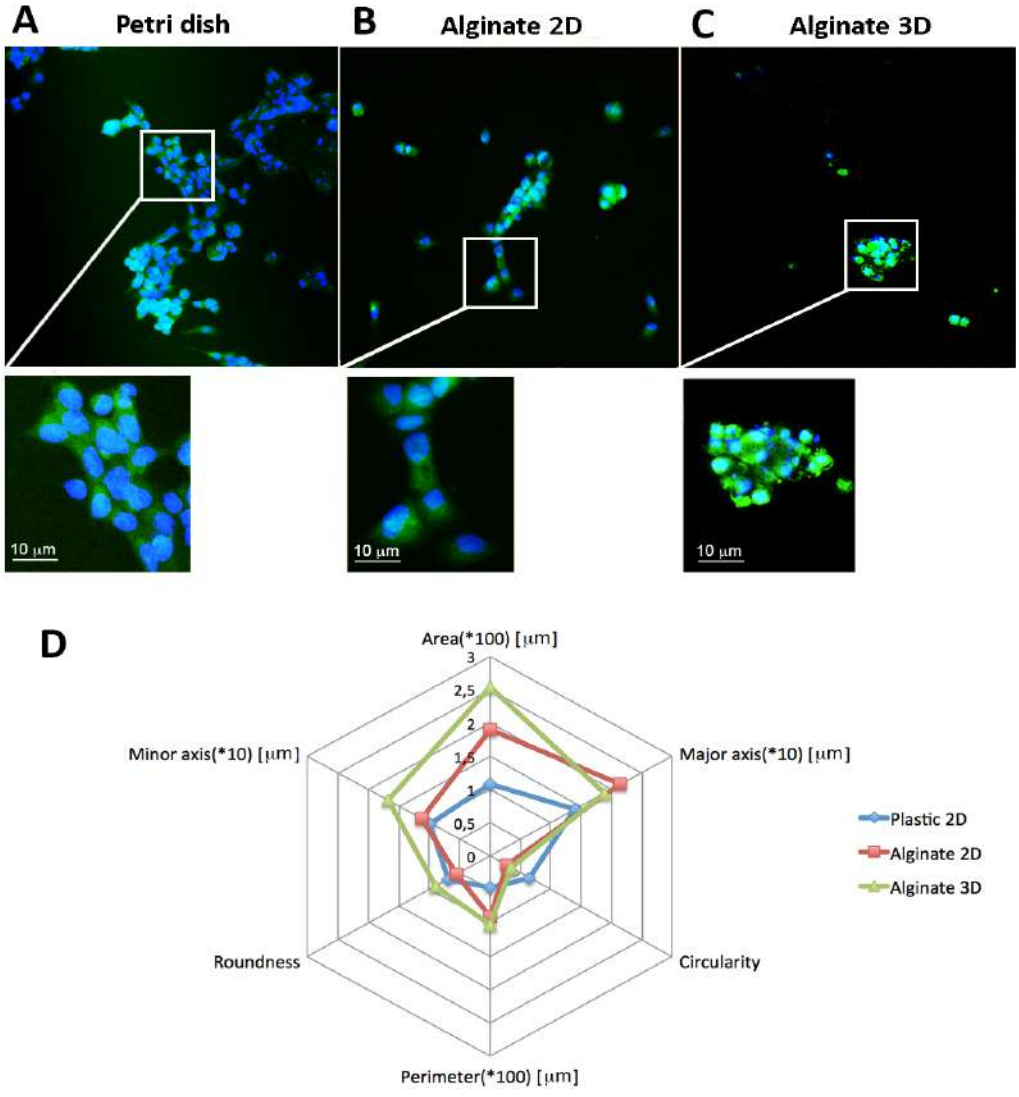

Figure 3.4: Cell morphology. Cells cultured on plastic (panel A), alginate-functionalized plastic (panel B) or embedded in 3D alginate hydrogels (panel C) show strongly different morphologies (blue: DAPI; green: Phalloidin). In particular, cells exhibit a flat shape in both 2D conditions; this morphology, even though selfexplanatory of a good cell adhesion,

heavily limits cell-to-cell contacts, which are maintained in 3D culture. Panel D shows quantitative information about cell morphologies in relation to their culture environment; in detail: area, perimeter, major axis, minor axis, circularity and roundness were analyzed for each culture condition. All the measures are expressed in μ m, except Roundness and Circularity, which are dimensionless (values ranging from 0 to 1).

3.3.5. Cell cluster formation

The presence of cell clusters was investigated in 3D gels by histological analysis of the gel inlets. For this analysis, only gels which had given the best cell viability results (i.e. 150-200 kPa, 300-350 kPa and 900-1800 kPa stiffness) were analysed. Initially, cells were distributed evenly as single cells inside each type of gel (data not shown). After 7 days, most of the cells within the hydrogels with low stiffness (150-200 kPa) proliferated to form spheroids with a mean size of 100 mm (Figure 5, panel A). In contrast, in stiffer gels, only a few cells composed the majority of clusters (Figure 5, panels B and C). After 14 days, the size of aggregates in cell laden gels with low stiffness increased to 300 μm (Figure 5, panel C); the cluster size remained almost constant in stiffer substrates (>300 kPa), where cells did not show similar proliferation ability (Figure 5, panels D and E).

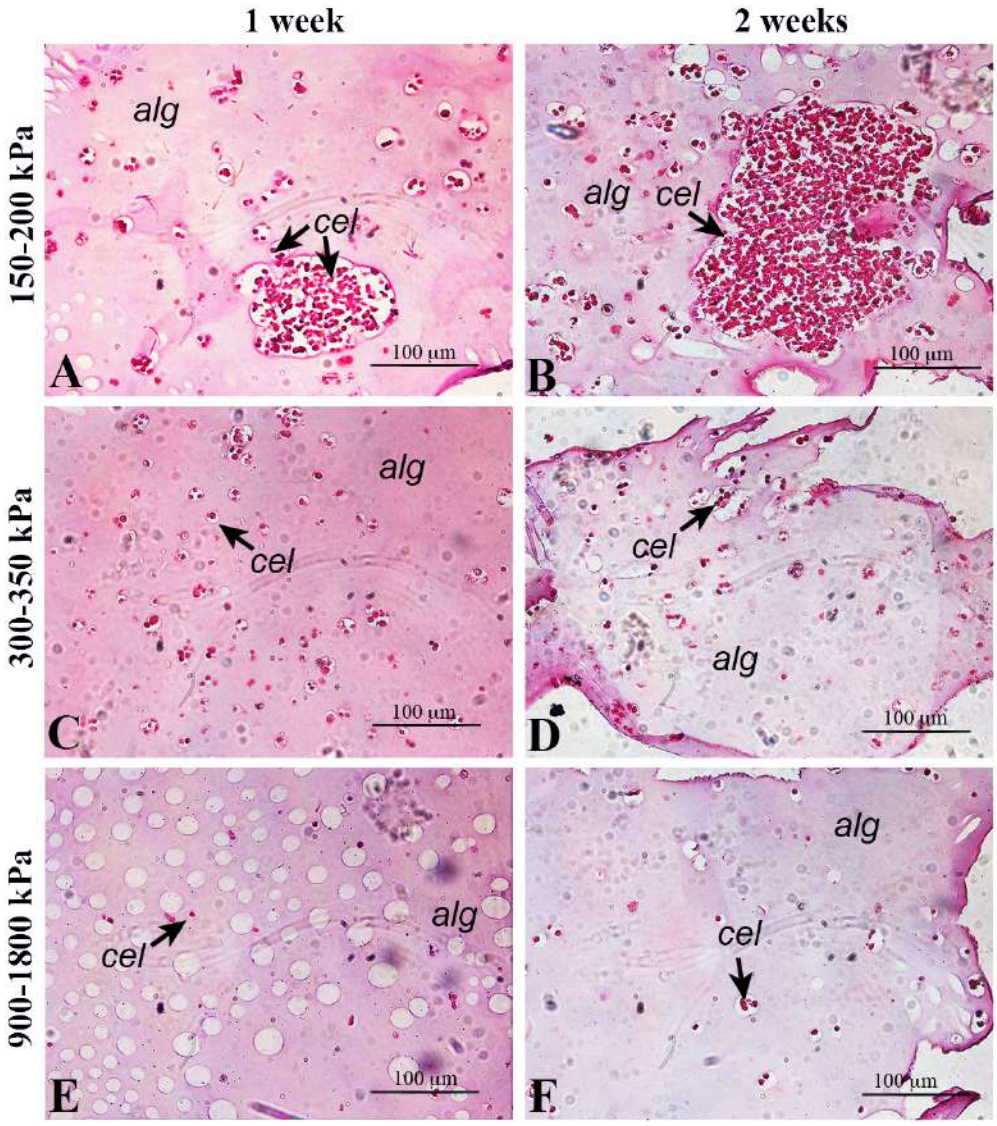

Figure 3.5: Cell proliferation and cluster formation. Histology of three alginate types (150–200 kPa, 300–350 kPa and 900–1800 kPa). Hematoxylin/eosin-stained sections are shown at 7 (left column) and 14 days (right column). Alginate (alg) is identified by the pink background, while cells (cel) are indicated by arrows and are purple. It is clearly observable that, if in stiff substrates cells are relatively isolated without significant proliferation rates both at 7 and 14 days (panels C, E and D, F, respectively), in soft gels they are highly proliferate, reaching clusters of 100 µm in one week (panel A) and 300 µm in two weeks (panel B).

The presence of clusters in relation to their dimensions was analysed for each type of gel. Results are shown in Figure 6. It can be observed that in moderately stiff (900-1800 kPa) and medium stiffness gels (300-350 kPa), clusters maintained small dimensions (<10 mm and about 30 mm, respectively) after both 1 and 2 weeks of culture. In contrast, in the softest gels (150-200 kPa), clusters reached greater dimensions (200 mm and > 250 mm after 1 and 2 weeks of culture, respectively), and the percentage of isolated cells decreased.

In soft cell laden alginates, together with a higher cluster dimension, we also observed higher values of cluster density, which passed from 56% (±3,6%) during the first week to 70% (±6,5%) in the second week (Table 2).

Chapter 4

3D in vitro model of highly aggressive breast cancer

4.1. Abstract

Purpose of this study was the development of a 3D material to be used as substrate for breast cancer cell culture. We developed composite gels constituted by different concentrations of Alginate (A) and Matrigel (M) to obtain a structurally stable-in-time and biologically active substrate. Human aggressive breast cancer cells (i.e. MDA-MB-231) were cultured within the gels. Known the link between cell morphology and malignancy, cells were morphologically characterized and their invasiveness correlated through an innovative bioreactor-based invasion assay.

A particular type of gel (i.e. 50% Alginate, 50% Matrigel) emerged thanks to a series of significant results:

1. cells exhibited peculiar cytoskeleton shapes and poly-nuclei organization characteristic of their malignancy;

2. for the first time in a 3D in vitro environment, cells expressed the formation of the so-called invadopodia, actin-based protrusion of the plasma membrane through which cells anchor to the extracellular matrix;

3. cells were able to migrate through the gels and attach to an engineered membrane mimicking the vascular walls hosted within bioreactor, providing a revolutionary 3D in vitro model of the very precursor steps of metastasis.

4.2. Materials and methods

4.2.1. Cell culture

Commercially available human MDA-MB-231 cells were used. MDA-MB-231 is an adherent cell line derived from pleural effusion of primary breast adenocarcinoma.

Cells were cultured in DMEM medium supplemented with 10% Fetal Bovine Serum (FBS) and 1% penicillin-streptomycin (P/S) (all from Sigma Aldrich), hereafter referred to as complete medium. Same cells were used both for 3D and 2D controls.

4.2.2. Tumour hydrogel preparation and culture

To prepare alginate solution, alginate powder (Manugel GMB, FMC BioPolymer) was mixed in physiological buffer at a concentration of 0.5% (w/v), as previously assessed [30]. Effective intimate mixing was guaranteed by exposing alginate solution for 12 hours under vigorous magnetic stirring at room temperature. Matrigel was thawed over night at 4 °C. Meanwhile, an agar solution at 1% (w/v) concentration was prepared by mixing Agar (DIFCO Laboratories) in physiological buffer enriched with 0.5 M of $CaCl_2$ (J. T. Baker). The solution was brought to the boil, poured into 6-well plates until ~1 cm height was obtained and allowed to cool until complete solidification. Holes of 0.5 cm diameter were then cut into the agar, using a Pasteur glass pipette, to make molds.

Cells were enzymatically detached from tissue plates and suspended in alginate solution. The suspension was moved to ice and Matrigel was added in variable quantity depending on the composite. Initially, we tested the following combinations: (i) 100% alginate (hereafter 100% A); (ii) 75% alginate and 25% Matrigel (hereafter 75%:25% A:M); 50% alginate and 50% Matrigel (hereafter 50%:50% A:M); 25% alginate and 75% Matrigel (hereafter 25%:75% A:M); 100% Matrigel (hereafter 100% M). The final cell density was 1 million/ml for all gel types.

To form a single gel, 100 μl of solution containing 100.000 cells were dispensed into agar molds using a tip. Gelation was allowed to take place at 37 °C for 1 hour and 15 minutes, in order to ensure the complete diffusion of calcium ions from agar to alginate solution and the thermally induced cross-linking of Matrigel.

Gels were gently removed from the molds, transferred into a 96 multi-well plate and maintained in complete medium containing 5 mM $CaCl_2$. Medium was changed every two days. A schematic representation of the protocol is shown in Figure 1, panel A.

4.2.3. Cell viability assay

After 24 hours, cellular response to gel interaction was investigated to prove the biocompatibility of the new composites. For this purpose, gels were washed with phosphate-buffered saline (PBS) and incubated with a Live/Dead staining (Live/Dead Cell Double Staining Kit, Sigma Aldrich) at 37 °C for 15 minutes. Gels were then imaged using an upright microscope equipped with transmitted illumination and epifluorescence (Eclipse Ni-U, Nikon) to

discriminate live cells (calcein AM stained-green) from dead cells (propidium iodide stained-red).

4.2.4. Histology

After 7 days, cell-laden hydrogels were processed for histological analysis in order to observe the level of intimate mixing of alginate and Matrigel in generating new composites and the distribution of cells within. Briefly, samples were dehydrated in ethanol scale, paraffin embedded, cross-sectioned (7 μm thick) at different levels and stained with Masson trichrome. Images were acquired by using a Nikon H550L optical microscope.

4.2.5. Confocal microscopy

To examine the morphology of cells within the gels, 3D samples were analysed by optical confocal laser-scanning microscopy. 2D plastic cultures and paraffin-embedded xenograft slices were used as controls.

3D gels were fixed with 4% paraformaldehyde after 1, 4 and 7 days.

Nuclei were stained with 1 μg/ml propidium iodide (PI), while actin filaments were stained with 100 μM Alexa Fluor 488 Phalloidin (both by Sigma-Aldrich). Before PI staining, gels were treated with 100 μg/ml Rnase for 30 minutes.

Images were acquired through a confocal laser-scanning microscope (Leica TCS SP5 AOBS) with a sequential image acquisition to avoid spectral cross-talk. Alexa Fluor 488 was excited with the 488 nm line of the Ar laser and its fluorescence was collected in a spectral window of 500 to 580 nm. For PI, 543 nm excitation wavelength and 600–700 nm spectral window emission were

used. For 3D gels, stacks comprising 100 optical sections, each with a 375×375-μm field of view and 512×512-pixel image matrix, were obtained through a depth of 100 μm.

Xenograft paraffin-embedded sections derived from orthotopic xenografts of MDA-MB-231 cells in mice were provided by the National Cancer Research Institute of Genoa (Italy). Shortly, Swiss nu/nu immunocompromised mice were purchased from Charles River (Calco, Como) and maintained in 12-hour dark/light cycles with water and food ad libitum. Animals were housed and maintained in the Animal Care Facility of the IRCCS San Martino-IST, accordingly to national and European regulations (D.L. 4/3/14 No. 26; 86/609/EEC Directive). All animal experiments were approved by the internal Ethic Committee and by the Italian Ministry of Health. A group of 27 six-week-old female mice were anesthetized with a mixture of Ketamine-Xylazine given intraperitoneally, the mammary fat pad of the inguinal fourth gland was exposed and 500.000 cells were injected in 10 μl of PBS using a disposable syringe with a 29 G needle. Animals were monitored daily and euthanized when tumors reached the size of 1200 mm^3 and before any sign of suffering became detectable. Tumors were removed and frozen for genomic analysis [31]. Sections of 50 μm were cut rehydrated, and stained with PI and Alexa Fluor 488 Phalloidin.

4.2.6. Image post-processing

In order to aid visualization of the arrangement of nuclei and actin filaments, the registered images were processed using the public domain NIH ImageJ program. Signals due to nuclei or actin filaments were separated from

that due to background on the basis of signal intensity and grey-scale morphology. The same program was used to obtain 3D rebuilding of gels by z-stack methodology.

4.2.7. Nuclei segmentation and quantification

Cell proliferation rate within 3D materials was obtained by counting the number of nuclei within the reconstructed confocal stacks. To do that, we adopted a protocol of nuclei segmentation developed by other authors [32], that combines the Lines-of-Sight (LoS) concept with a local adaptive pre-processing to separate apparently touching cell nuclei into approximately convex parts representing single cell nuclei. Numbers of nuclei at days 4 and 7 were finally normalized on nuclei at day 1, in order to be presented as proliferation rates. The procedure of nuclei segmentation is schematically represented in Figure 3, panel B.

4.2.8. Size and shape cell analysis

Confocal images were analysed by ImageJ to measure and quantify several features characterizing cells growing in 3D conditions. In particular, we considered cell area, perimeter, major axis and minor axis lengths.

We finally defined two parameters to evaluate the grade of irregularity and elongation of cell cytoskeleton:

$$Form\ Factor\ (FF)\ =\ \frac{Area}{Perimeter^2} \qquad (1)$$

$$Elongation\ Index\ (EI)\ = \frac{Major\ Axis}{Minor\ Axis} \qquad (2)$$

For a perfect circle (cell with round shape) the FF value tends to $\frac{1}{4\pi}$.

4.2.9. Electrospinning of polycaprolactone membranes and scanning electron microscopy (SEM)

Electrospun membranes were produced by dissolving polycaprolactone (PCL) in 1:1 absolute ethanol:chloroform (Bio-Optica) to create a 20% (w/v) final solution. The polymer solution was loaded into a syringe (12 ml), and a 21 Gauge needle was attached. The syringe was securely fitted to a syringe pump-driver (Harvard Apparatus PHD 2000). The needle tip was connected to a high voltage power source (Gamma High Voltage ES50P-10W) operating at 7 kV [33] and positioned 12 cm from the collection plate (covered with an aluminium foil) [34]. The PCL solution was delivered at a constant flow rate of 2 ml/hour for 4 h. Finally, the membranes were air-dried for 24 h to allow residual solvent to evaporate.

The microstructure and porosity of PCL membranes were evaluated with a scanning electron microscope (SEM Hitachi 2500) after metallization with gold by using a Polaron SEM coating system.

4.2.10. Assembly of tumour hydrogel and membrane within bioreactor for recapitulating the metastatic condition

The set-up for cell intravasation was assessed by using the multi-organ bioreactor by React4life S.r.l. (www.react4life.com). The peculiarity of this system is the possibility to host 3D engineered tissues strictly in contact with a

porous membrane, eventually functionalized to better mimic the blood vessel environment.

The previously described electrospun membranes were sterilized by irradiating with ultraviolet (UV) light at a distance of 10 cm over night; after that, they were sterilely placed between two polycarbonate rings to define the useful experimental area, pre-conditioned by pipetting 1% w/v gelatine solution in PBS above and incubated for 15 minutes. Finally, gelatine coating was removed and membranes were washed in PBS.

One membrane per experiment was placed within the multi-organ bioreactor. The tumour hydrogel was placed in the upper part of the bioreactor in contact with the membrane, to allow cells escaped from the gel to functionally attach to the membrane and to eventually enter in the bottom part of bioreactor, that is connected to a fluidic circuit enabling their collection.

The cellular migration and intravasation was monitored by confocal sectioning on the membrane after 3 days.

4.3. Results

4.3.1. Composite hydrogel assessment

Hydrogel initial compositions (i.e. 100% A, 75%:25% A:M, 50%:50% A:M, 25%:75% A:M, 100% M) were firstly assessed from a structural point of view. Hydrogels belonging to 25%:75% A:M and 100% M categories did not show a proper robustness and structural stability and thus were immediately excluded (Figure 1, panel B). The other three categories were chosen as

substrates for 3D cell culture. Initially, gels of 100 µl were loaded with 200.000 cells each one; however, this concentration caused a fast degradation of the 50%:50% A:M category (Figure 1, panel C). To our knowledge of the current literature, this behaviour may be caused by the action of the metal-protease MT-MMP, necessary for cell proliferation and for the integrin-mediated invasion process. To solve these issues, already expressed in some works in literature [35], we adopted two different strategies: first, cell density was reduced from 200.000 to 100.000 per gel, ensuring a still good cell-to-cell contact. Secondly, we functionalized the bottom of the culture plate with a thin layer of Matrigel before moving gels into, as suggested by Lee et al. [36].

Under these conditions, stable gels for the whole experimental period were obtained (Figure 1, panel D).

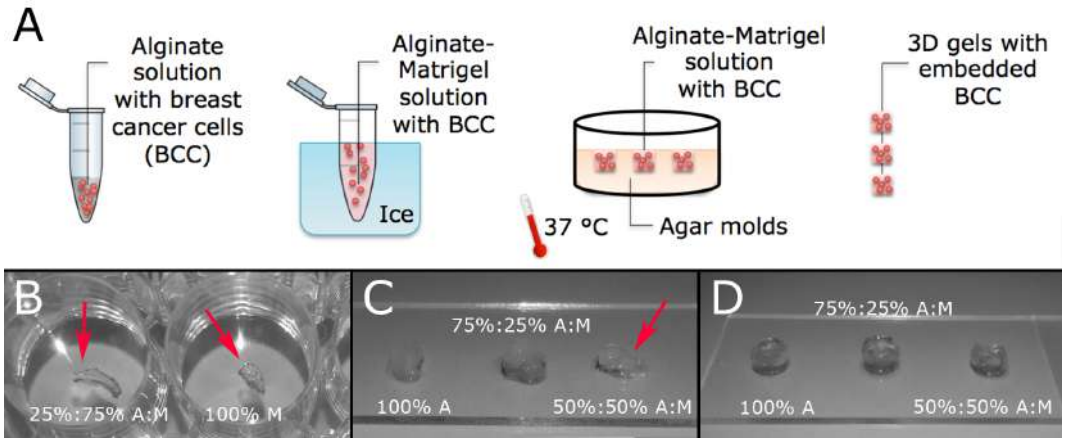

Figure 4.1: Composite cell-laden gel development. a) Schematic description of the protocol used to produce 3D cell-laden Alginate-Matrigelcomposite gels: breast cancer cells MDA-MB-231 are seeded first in liquid alginate and then Matrigel is added working on ice. The cell-laden solution is transferred into Agar molds enriched with CaCl2 ions at 37 °C for to allow gelation. Then, 3D gels are removed by molds and trasferred into plates with culture media. b) Gels composed by 25%:75% A:M and

100% M ratios resulted too soft and not handy. c) a concentration of 2 million cells/ml caused a fast degradation of 50%:50% A:M gels, thus it was reduced to 1 million cells/ml. d) finally, structurally compact gels were obtained.

Immunohistological staining (trichrome) and imaging of MDA-MB-231 cells embedded within the three different composite materials highlight the good intimate mixing of Matrigel and Alginate (the color of substrates tends to green increasing Matrigel content, as shown in Figure 2).

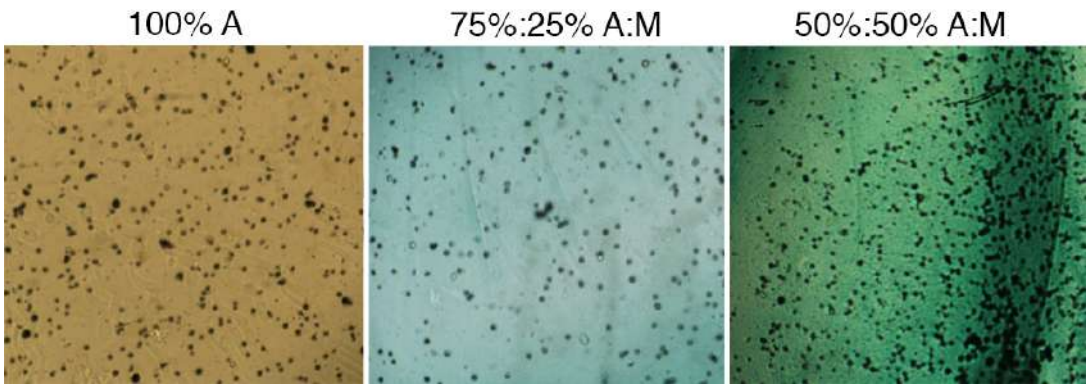

Figure 4.2: Histological analysis. - Immunohistological staining (trichrome) and imaging of MDA-MB-231 cells (black) embedded within the three different composite materials. The color of substrates tends to green increasing Matrigel content.

4.3.2. High viability and cell proliferation within gels

Tumor cells in the hydrogels demonstrated high viability and density (Figure 3, panel A) also in the inner parts of materials and time-dependent growth consistent with observations from confocal images (Figure 3, panel C), validating our gelation protocol and gel mass transport properties. Although

initial cellular proliferation in gels on day 4 was marginally low, it recovered to above 4 fold change relative to the initial cell number on day 7.

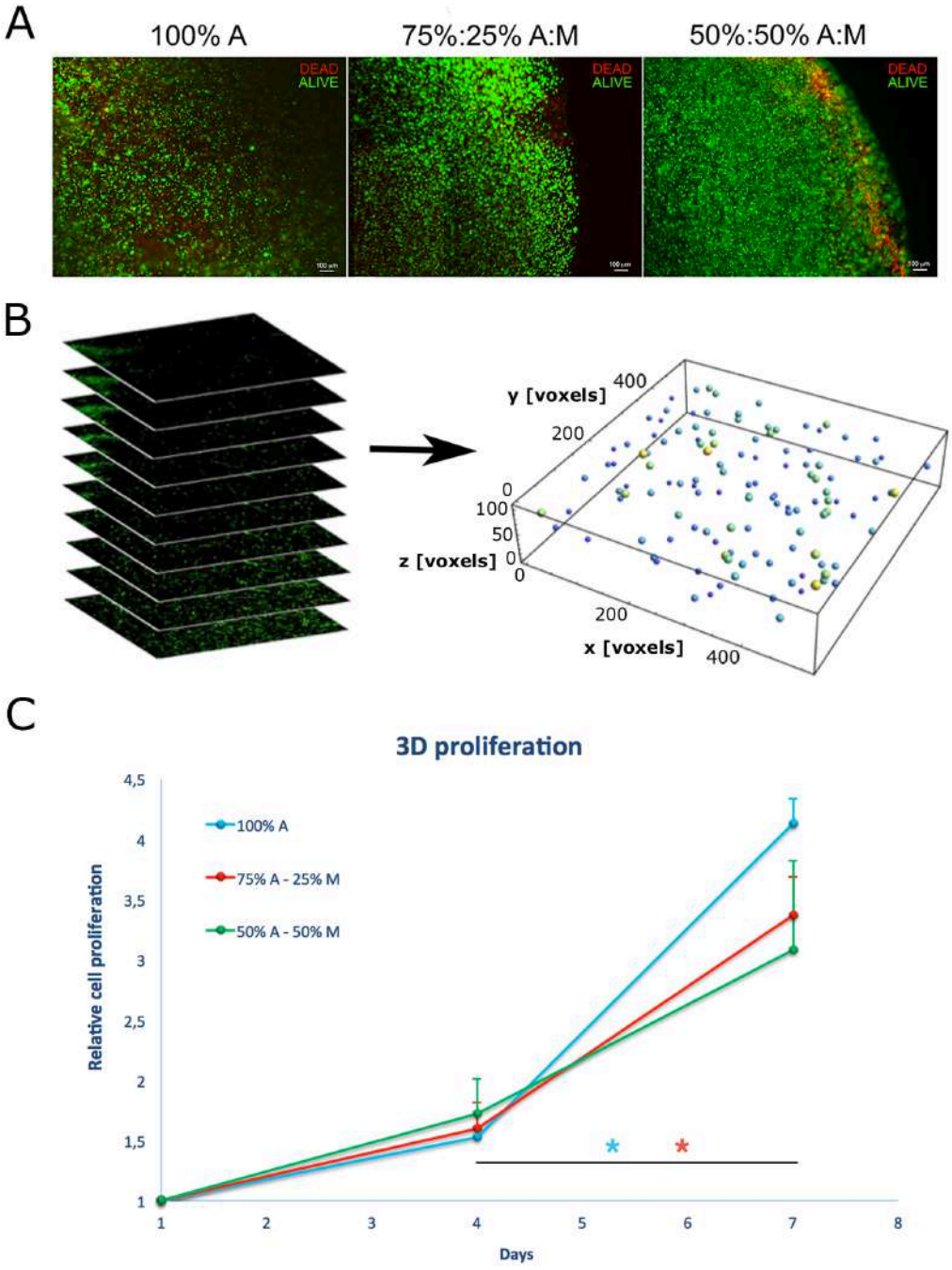

Figure 4.3: Cell viability and proliferation. a) MDA-MB-231 cells cultured with materials for 24 h, stained with fuorescence dyes: calceinAM (green) for live cells and propidium iodide (red) for dead cells. b) procedure for nuclei segmentation to count cell number within different materials at different time points c) MDAMB- 231 cell proliferation obtained by nuclei segmentation

after4 and 7 days of culture for different materials. Symbol * indicates statistical significance (t-test, $P<0.05$).

4.3.3. Cell morphology: polinuclei, invadopodia, cytoskeleton irregularity and elongation

Cell morphology was firstly qualitatively assessed. Both in 2D and *in vivo* (xenograft) conditions, MDA-MB-231 cells expressed, as expected, their typical elongated and stellate morphology (Figure 4, panels A and B).

Trying to obtain a similar conformation also in a 3D environment, we analyzed cell morphology within the three different categories of gels at three different time points (1, 4 and 7 days).

In alginate gels, cells maintained a round morphology, typical of suspension phase and expressive of a non-malignancy condition, regardless of time point (Figure 4, panels C, D, E); in presence of Matrigel, cells tended to elongate, accordingly to their aggressiveness (Figure 4, panels F to K). More interestingly and in contrast to 2D controls, in the same gels we observed a poly-nuclei conformation, known to be linked to malignancy as well. Indeed, while nuclei assumed a round and regular shape in 100% A gels (Figure 4, panel L), they showed a multiple and jagged conformation in presence of Matrigel (Figure 4, panels M and N). Finally, only in 50%:50% A:M gels, we observed manifestation of invadopodia (Figure 4, panels I to K), actin-based protrusion of the plasma membrane through which cancer cells anchor to the Extracellular Matrix and degrade it. This feature, never observed in a 3D *in vitro* environment, was expressed by MDA-MB-231 in the same gels regardless of time point.

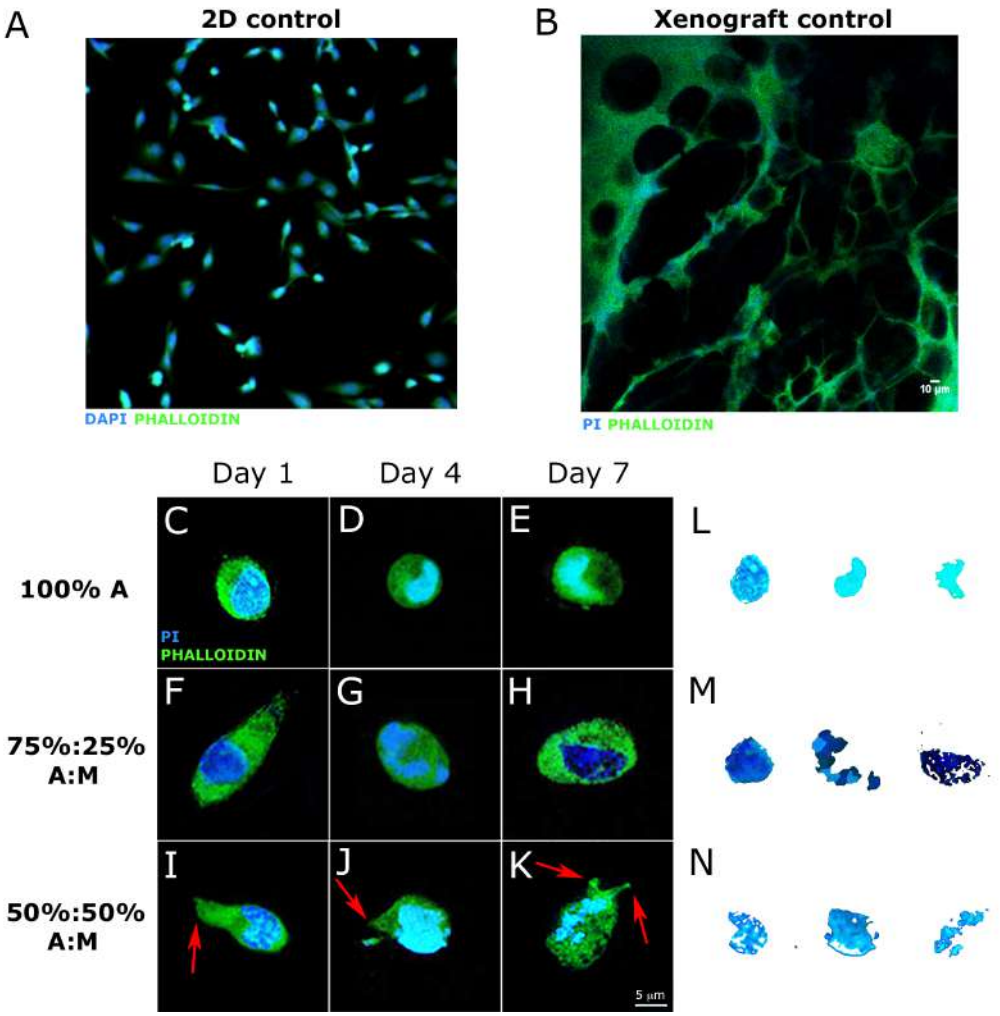

Figure 4.4: Cell morphological characterization. a) Morphology of MDA-MB-231 breast cells cultured in two-dimensions. Cells were stained for F-actin (phalloidin) and nuclei were counterstained with DAPI; cells show a stellate morphology. b) Confocal section of representative xenograft implant of MDA-MB-231. Cells were stained for F-actin (phalloidin) and nuclei were counterstained with Propidium Iodide. Cells show elongated/stellate morphology. c)-k) Confocal sections of representative cells embedded within Alginate/Matrigel composite gels at different time points (1, 4 and 7 days). Cells were stained for F-actin (phalloidin) and nuclei were counterstained with Propidium Iodide. Cells show round morphology in 100% A gels, thus not expressing their spreading capability; they show elongated morphology in 75%:25% A:M gels; they finally show stellate morphology and invadopodia (red arrows) in 50%:50% A:M gels. l-n) Nuclei shapes isolated from c-to-k panelsvshow that in presence of Matrigel cells express poly-nuclei conformation, characteristic of malignancy.

From a quantitative point of view, gels containing a Matrigel component showed morphological features closer to elongated cells cultured in 2D conditions (Figure 5, panel B). Irregularity (Figure 5, panel C) and elongation (Figure 5, panel D) resulted proportional to Matrigel content, highlighting that 50%:50% A:M gels are the most permissive to cell arrangement and organization in a 3D environment. In detail, irregularity is inversely proportional to Form Factor, since a value of Form Factor closer to $\frac{1}{4\pi}$ means that cells exhibit a most regular shape.

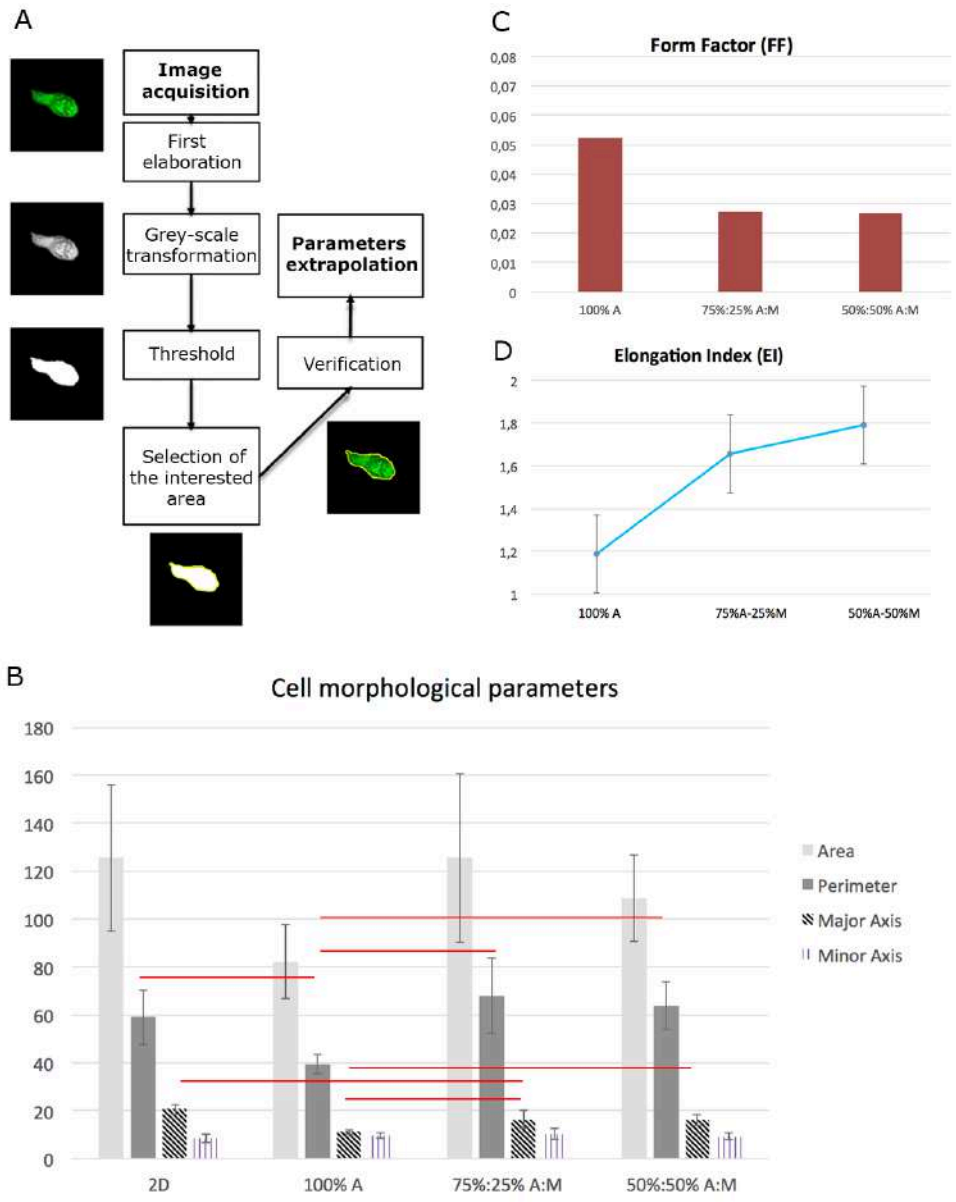

Figure 4.5: Morphological parameters extrapolation. a) The extrapolation of cell morphological parameters follows different main steps. In the first step (top), images are adjusted through a series of transformation, i.e. grey-scale transformation and threshold. The area of the cell is then automatically selected, but a manual check is done by overlapping cytoskeleton (actin) image. Finally, parameters such as area, perimeter, major and minor axes are automatically extrapolated by the software. b) Area, Perimeter, Major Axis and Minor Axis (averages, standard deviation) of cells cultivated on 2D substrates and within the composite gels. Red lines mean statistical significance (t-test, $P<0.05$). c) Irregularity Factor (IF) for cells within the gels. Higher the IF, greater the irregularity of cell shape d) Elongation Index (EI) for cells within the gels. Higher the EI, greater the elongation of cell shape.

4.3.4. Cell motility in bioreactor

After 3 days in culture, membranes were removed from bioreactor and analysed under microscope to observe the presence of entrapped cells. While we did not observe any cells in matrices corresponding to 100% A gels, our results show that both in 75%:25% A:M and in 50%:50% A:M cells were able to migrate through the gels, escape from them and adhere to the porous electrospun PCL-gelatine membranes (Figure 6, panels C to F), confirming these materials as permissive substrates for the study of 3D tumour cell invasion in vitro.

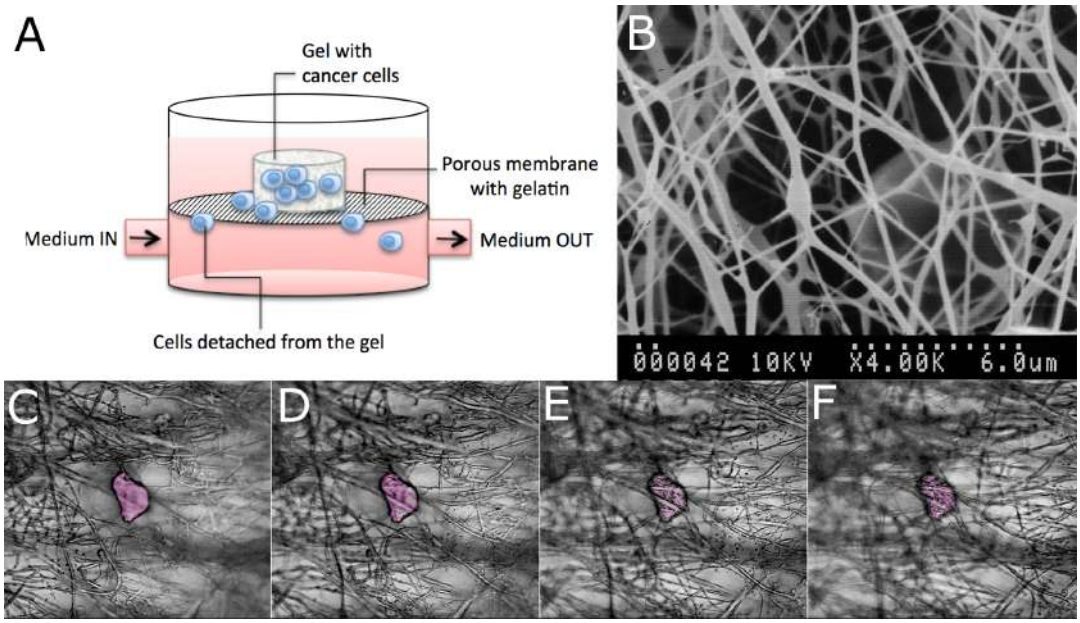

Figure 4.6: Preliminary steps of metastasis in bioreactor. a) Schematic representation of the set-up for observation of cell spread and intravasation. Bioreactor was developed by React4life S.r.l. b) Electrospun membrane used to mimick blood vessel interface. The membranes were realized in polycaprolacton (PCL) by electrospinning technique. c-f) Confocal slides of cell entrapped within the membrane (cell is in false colours).

4.4. References

1 Cavo, M. *et al*. Microenvironment complexity and matrix stiffness regulate breast cancer cell activity in a 3D in vitro model. *Scientific reports* **6** (2016).

2 Khanna, C. & Hunter, K. Modeling metastasis in vivo. *Carcinogenesis* **26**, 513-523 (2005).

3 Pampaloni, F., Reynaud, E. G. & Stelzer, E. H. K. The third dimension bridges the gap between cell culture and live tissue. *Nature reviews Molecular cell biology* **8**, 839-845 (2007).

4 Kim, J. B. in *Seminars in cancer biology*. 365-377 (Elsevier).

5 Horch, R. E. *et al*. Cancer research by means of tissue engineering–is there a rationale? *Journal of cellular and molecular medicine* **17**, 1197-1206 (2013).

6 Burdett, E., Kasper, F. K., Mikos, A. G. & Ludwig, J. A. Engineering tumors: a tissue engineering perspective in cancer biology. *Tissue Engineering Part B: Reviews* **16**, 351-359 (2010).

7 Hutmacher, D. W. *et al*. Translating tissue engineering technology platforms into cancer research. *Journal of cellular and molecular medicine* **13**, 1417-1427 (2009).

8 Puguan, J. M. C., Yu, X. & Kim, H. Characterization of structure, physico-chemical properties and diffusion behavior of Ca-Alginate gel beads prepared by different gelation methods. *Journal of colloid and interface science* **432**, 109-116 (2014).

9 Weiswald, L.-B., Bellet, D. & Dangles-Marie, V. Spherical cancer models in tumor biology. *Neoplasia* **17**, 1-15 (2015).

10 Godugu, C. *et al*. AlgiMatrix™ based 3D cell culture system as an in-vitro tumor model for anticancer studies. *PloS one* **8**, e53708 (2013).

11 Kenny, P. A. *et al*. The morphologies of breast cancer cell lines in three - dimensional assays correlate with their profiles of gene expression. *Molecular oncology* **1**, 84-96 (2007).

12 Kleinman, H. K. & Martin, G. R. in *Seminars in cancer biology*. 378-386 (Elsevier).

13 Shaw, L. M. Tumor cell invasion assays. *Cell Migration: Developmental Methods and Protocols*, 97-105 (2005).

14 Albini, A. *et al*. A rapid in vitro assay for quantitating the invasive potential of tumor cells. *Cancer research* **47**, 3239-3245 (1987).

15 Kenny, P. A. *et al*. The morphologies of breast cancer cell lines in three-dimensional assays correlate with their profiles of gene expression. *Molecular oncology* **1**, 84-96 (2007).

16 Hotary, K., Li, X.-Y., Allen, E., Stevens, S. L. & Weiss, S. J. A cancer cell metalloprotease triad regulates the basement membrane transmigration program. *Genes & development* **20**, 2673-2686 (2006).

17 Lee, G. Y., Kenny, P. A., Lee, E. H. & Bissell, M. J. Three-dimensional culture models of normal and malignant breast epithelial cells. *Nature methods* **4**, 359 (2007).

18 Albini, A. & Benelli, R. The chemoinvasion assay: a method to assess tumor and endothelial cell invasion and its modulation. *Nature protocols* **2**, 504-511 (2007).

19 Bharadwaj, S., Thanawala, R., Bon, G., Falcioni, R. & Prasad, G. L. Resensitization of breast cancer cells to anoikis by tropomyosin-1: role of Rho kinase-dependent cytoskeleton and adhesion. *Oncogene* **24**, 8291 (2005).

20 Amaro, A. *et al*. A highly invasive subpopulation of MDA-MB-231 breast cancer cells shows accelerated growth, differential chemoresistance, features of apocrine tumors and reduced tumorigenicity in vivo. *Oncotarget* **7**, 68803 (2016).

21 Mathew, B. *et al*. Robust and automated three-dimensional segmentation of densely packed cell nuclei in different biological specimens with Lines-of-Sight decomposition. *BMC bioinformatics* **16**, 187 (2015).

22 Deitzel, J. M., Kleinmeyer, J., Harris, D. E. A. & Tan, N. C. B. The effect of processing variables on the morphology of electrospun nanofibers and textiles. *Polymer* **42**, 261-272 (2001).

23 Khil, M. S., Cha, D. I., Kim, H. Y., Kim, I. S. & Bhattarai, N. Electrospun nanofibrous polyurethane membrane as wound dressing. *Journal of Biomedical Materials Research Part B: Applied Biomaterials* **67**, 675-679 (2003).

Chapter 5

A novel bioreactor combined with single cell analysis allows recapitulating preliminary steps of metastasis paradigm *in vitro*

5.1. Abstract

Metastasis process plays a key role on the prognosis of breast cancer, but lots of aspects are still unanswered.

In this work, we combined a bioreactor-based bioengineering approach with single cell analysis of Circulating Tumor Cells (CTCs). Analysis of human CTCs has now revealed important features of cancer metastasis, such as the high metastatic potential of CTC-clusters compared to single CTCs. For this reason, we applied the same approach to our in vitro system. Single cell qPCR of the circulating LM2 cells was performed. A proof-of-concept that the approach can work was performed, as well as evidence that the cells can be extracted from the device and used for molecular analysis.

5.2. Materials and Methods

5.2.1. Experimental set-up

MOOD (Multi-Organ On Device) bioreactor by React4life S.r.l. is composed by a main chamber, subdivided into two units by a membrane. The membrane is interchangeably, thus different membranes can be used according to the experiment. Three-way valves connecting Marprene oxygen-permeable tubes provide an easy replacement of the culture medium. The overall system is governed by a commercial peristaltic pump. The described set-up works into a standard humidified incubator at 37 °C and 5% CO_2.

To recreate two physically independent environments (i.e. the primary tumour environment and the metastatic one) we used two bioreactors set in series. Of the two bioreactors used, the first one hosted a 3D engineered breast tumour and a membrane allowing detached cells entering in circulation; the second one hosted a second membrane, allowing circulating cells to enter into the "metastatic chamber". The first chamber and the fluidic circuit were loaded with DMEM enriched with 1% FBS and 1% pen/strept, while the second/metastatic chamber was loaded with DMEM enriched with 10% FBS and 1% pen/strept, thus creating a serum gradient to improve cell motility.

The fluid velocity was set to $0.7\times10^{-3}\ \frac{m}{s}$ (capillary blood average speed).

The cellular migration and intravasation was monitored by removing the medium every 24 hours and counting the circulating cells into the different circuits (main and metastatic).

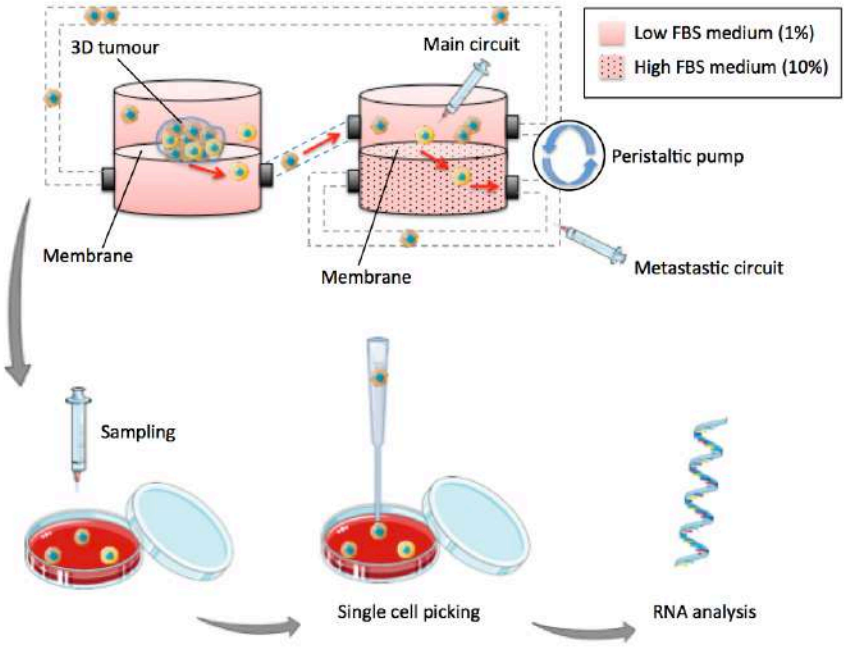

Figure 5.1: Schematic representation of the whole experiment. Two MOOD bioreactors are set in series to recreate both the intravasation and the extravasation processes. In the first MOOD, a 3D cell-laden gel is hosted as primary tumour model, in contact with the first membrane, so that cells can detach from the gel and enter in circulaton. Every 24 hours, media is sampled and replaced both from the main and the metastatic chamber. Cell counting is performed, then some cells are picked and analyzed.

5.2.2. Membrane development

Electrospun polycaprolactone (PCL)-based membranes were produced to be adopted as interfaces (both between the primary tumour and the fluidic circuit, and the fluidic circuit and the metastatic chamber). PCL ensures mechanical robustness to the membrane besides good biocompatibility; electrospinning technique allows obtaining highly porous matrices with various pore sizes ranging, firstly allowing an easy nutrient transport, secondly resulting permissive to cell migration[37].

To this aim, a custom-made electrospinning set-up was used. A solution of PCL (440744 by Sigma-Aldrich) at 20% w/v in chloroform/ethanol (1:1 v/v) mixture was realized and transferred to a 6 ml syringe connected to a 21 Gauge blunt tipped needle, as suggested by other authors[38]. The tip-to-collection plate (covered with aluminium foil) distance was 12 cm[34]. The needle tip was connected to a high voltage power source (Gamma High Voltage ES50P-10W) operating at 7 kV[33], and the polymer solution was feed into the needle at a rate of 2 ml/h by a syringe pump (Harvard Apparatus PHD 2000). The PCL membranes were detached and glued by a silicon-like glue to the inferior side of the disc in order to cover the hole and left in ventilate environment to dry over night. Membranes were detached after 5 hours of deposition and functionalized with a gelatin coating just prior to use. Gelatin-coated membranes are known to promote cell attachment[39], so this functionalization was adopted to attract escaping breast cancer cells from the primary tumour. The coating was realized on the top of the membrane by covering the PCL layer with 1% w/v gelatin (Gelatin from bovine skin, G9391, Sigma Aldrich) solution in phospate buffered saline (PBS). The solution was allowed to penetrate the PCL structure for 20 minutes at 37 °C; after this time, the exceeding gelatin was removed by a pipette. The described membranes were sterilized by irradiating with ultraviolet (UV) light at a distance of 10 cm over night; after that, they were placed in bioreactor. The tumour hydrogel was placed in the upper part of the bioreactor in contact with the membrane, to allow cells escaped from the gel to functionally attach to the membrane and to eventually enter in the bottom part of bioreactor, that is connected to a fluidic circuit enabling their collection.

5.2.3. Scanning electron microscopy (SEM)

Membrane porosity and morphology were examined by scanning electron microscopy (SEM). To this aim, samples taken from membranes were gold and a Hitachi S2500 SEM was employed. Images were acquired at 3.90K magnification.

5.2.4. Cell culture

MDA-MB-231 LM2 (herein referred to as LM2) cells are a derivative of MDA-MB-231 cells (breast adenocarcinoma) selected for their ability to metastasize to lung tissue in vivo. LM2 were expanded in Dulbecco's modified Eagle's medium (DMEM) enriched with 10% Fetal Bovine Serum (FBS) and 1% penicillin/streptomycin (all from Sigma Aldrich). When the required confluence was reached, cells were detached with 1X trypsin.

5.2.5. 3D breast tumour model

As primary breast tumour model, we developed fibrin-based cell-leaden hydrogels, realized as follows. For a single gel of 100 ml, a solution of HEPES (17,7 ml) and fibrinogen (32,3 ml) was prepared (solution A). As cross-linking solution (solution B), we mixed a CaCl2-based buffer (20 ml) with 3 ml of thrombin and 1,5 ml of Factor XIII. Solution B was allowed to mix at 37 °C for 30 minutes, then 25,5 ml of HEPES were added (solution C). 1 million of LM2 cells were suspended in solution A (50 ml), then solution C (50 ml) was added. The resultant was speedily mixed and deposited on a silicone mold, then incubated for 15 minutes to allow gelification.

Gels were washed into PBS solution in order to remove superficial, already detached cells and then were put within the bioreactor (one gel per experiment), in contact with the membrane.

5.2.6. Live/dead cell analysis and microscopy

Just after jellification, gels were incubated with a Live/Dead assay (Live/Dead Cell Double Staining Kit, Sigma Aldrich) at 37° C for 15 minutes to analyse cell viability and distribution. The 3D gel was imaged by using an upright microscope equipped with transmitted illumination and epifluorescence (Eclipse Ni-U, Nikon) to discriminate alive cells (calcein AM stained-green) from dead cells (propidium iodide stained-red).

5.2.7. Fluid dynamic model

In order to identify the best working conditions within the bioreactor, a physical model of the dynamic forces acting on circulating cells was carried out. In particular, we evaluated if the imposition of the capillary blood average speed ($0.7\times10^{-3}\ \frac{m}{s}$) within the bioreactor could allow cells to flow within the circuit without sedimenting.

To do this, we considered a single cell immersed in a liquid having rheological properties similar to the medium culture. In this context, the forces acting on the cell are: the gravity force F_g, the Archimedes force F_A and the Stokes force F_S, respectively defined as:

1) $$F_g = m\times g$$

where m is the cell mass and g is the gravity acceleration;

2) $$F_A = g\times\rho\times V$$

where g is the gravity acceleration, ρ is the fluid density and V is the cell volume;

3) $$F_S = 6\pi \times \mu \times r \times v$$

where μ is the fluid viscosity, r is the cell radium and v is the velocity of the cell within the fluid; v is the only variable of the three equations, and it can be imposed at the peristaltic pump level.

By substituting the variables with their known values, we obtain:

$$F_g = 9.8 \times 10^{-12} \ \frac{m}{s^2} \times kg = \ 9.8 \times 10^{-12} \ N$$

$$F_A = 9.8 \times 10^3 \times 5.2 \times 10^{-16} \ \frac{m}{s^2} \times \frac{kg}{m^3} \times m^3 = 5.1 \times 10^{-12} \ N$$

$$F_S = 6 \times 3.14 \times 10^{-4} \times 10^{-5} \times 0.7 \times 10^{-3} = 1.3 \times 10^{-11} \ N$$

By comparing the three values of the forces, we can see that the Stokes force is slowly predominant respect to the other forces. Consequently, cells circulating within the fluid and subjected to a capillary-like speed will tend to flow within the system rather than to deposit.

5.2.8. Cell counting and picking

After sampling from bioreactor, the material was transferred to low suspension 6-well plates. The very limited amount of cell material involved in metastatic studies required the use of a single cell manipulator. Cell picking was performed through the use of a CellCelector robotic system (ALS, Automated Lab Solutions) for semi-automatic single cell micromanipulation. This consists of an inverted microscope combined with micropipettes movable through motorized mechanical stages. Micropipettes are made of ultrathin glass capillaries coupled to an aspiration unit.

Firstly, a scanning of the whole source plate was performed in order to detect, select and count the number of cells and to acquire single cell or clusters images. Then, via microscope observation, specific cell were selected and aspirated by applying suction to the capillary micropipette. The aspirated liquid volume including the selected cell was transferred to a collection tube, where it was released by dispensation, in RNA buffer and conserved at -80 °C.

5.2.9. RNA analysis

LM2 cells were transfected with siRNA and were treated 24 h later with or without TGF 1 or SB-431542 for an additional 24 h. Total RNA was purified using Quick-RNA MiniPrep kit, and cDNA synthesis was performed using 1 g RNA and iScript cDNA synthesis kit (Bio-Rad) according to manufacturer's protocol. qPCR was performed using Fast SYBR Green enzyme (Applied Biosystems) and measured on ViiA 7 real time PCR system (Applied Biosystems). Transcript levels were analyzed using the Ct method.

5.3. Results

5.3.1. Membrane characterization

Fig. 2 shows images of membranes realized with a deposition of 5 hours. This deposition time allows obtaining membranes that are both structurally resistant and porous enough to allow cell migration into the thickness direction of the membrane.

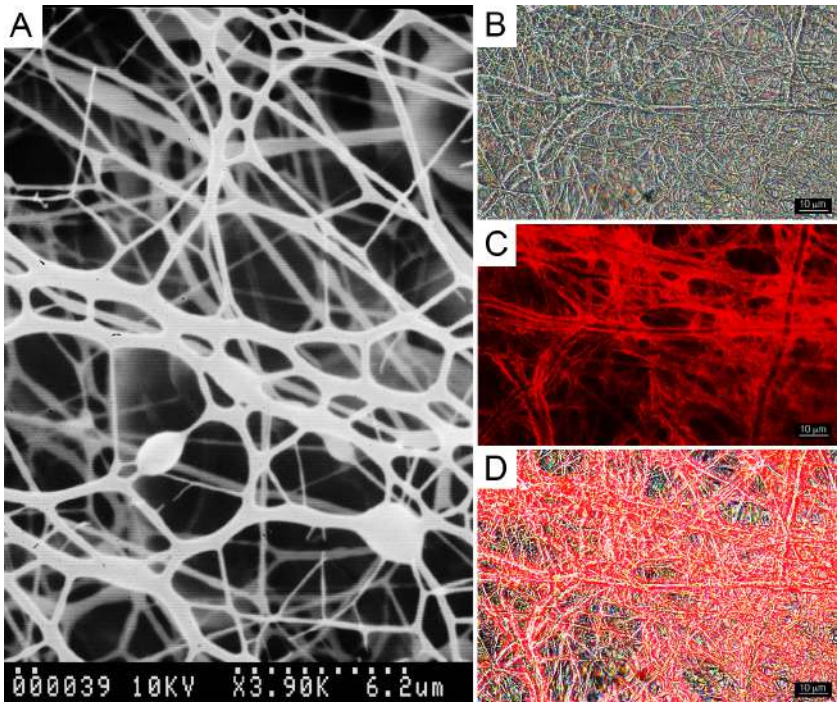

Figure 5.2: A) SEM image of the electrospun membanes (scale bar: 6.2 mm). B) Optical microscopy image of the same membrane (brightfield; scale bar 10 mm). C) Optical fluorescence microscopy image of the same membrane (gelatine is auto-fluorescent in red). D) Merge of panels B and C.

5.3.2. Engineered breast tumor

The adopted protocol produced 3D fibrin-based gels (Fig. 5, panel A). The cell-laden gels were cultured in bioreactor up to 48 hours (Fig. 5, panel B). Fig. 5, panel C, show cell distribution within the gel by optical microscopy; as visible, cells are distributed along the whole area of the material, while they appear greater or smaller basing on their position along the gel height. Images of the gels stained with the Live/Dead reagent show that there were many live/viable cells and that cells uniformly covered the majority of the surface area of the gels.

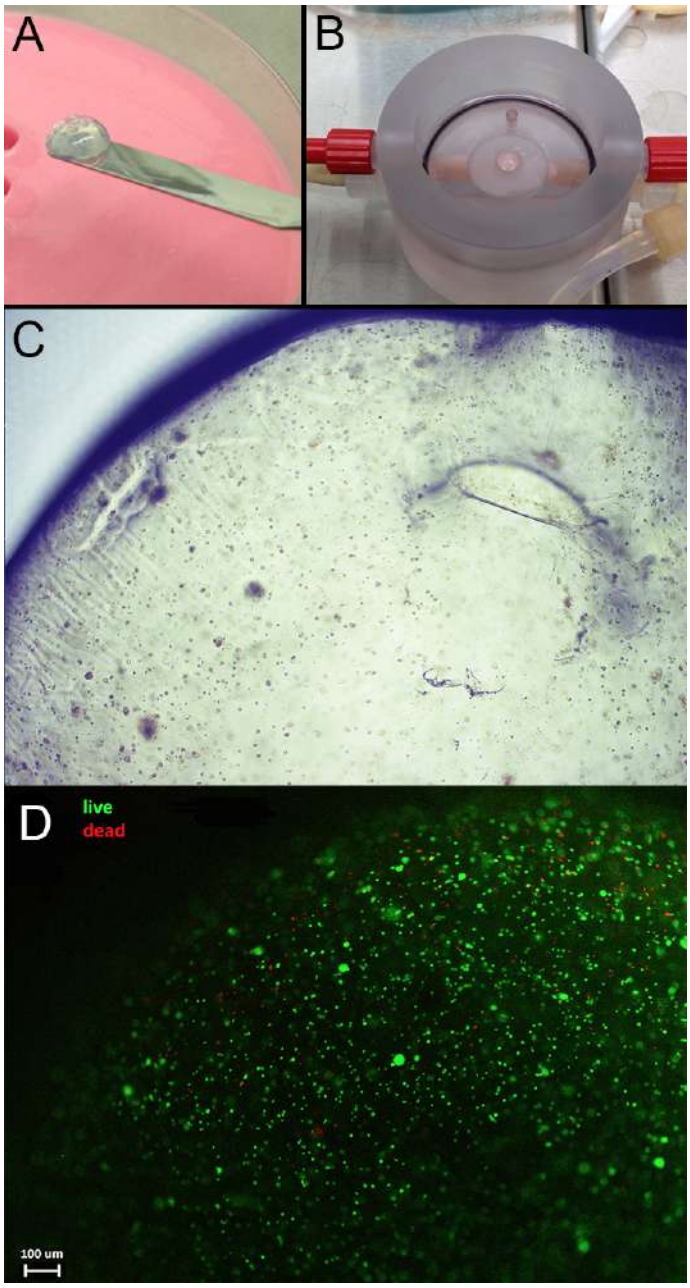

Figure 5.3: A) Fibrin-based gels with embedded LM2 cells just after jellification. B) MOOD bioreactor with the gel inside the camber. C) Optical microscopy image (brightfieldI) of the cell-laden gel. D) Optical fluorescence microscopy image of the cell-laden gel, stained with Dead/Alive kit (green: live cells; red: dead cells). Scale bar: 100 mm.

5.3.3. Set-up assessment

The set-up, consisting of 2 MOOD bioreactors connected in series, oxygen-

permeable Marprene tubes, three-way valves for sampling/replacement of culture medium, two electrospun membranes housed inside the bioreactor chambers and an engineered fibrin-based artificial tumour, was placed in an incubator at controlled temperature and humidity for 2 days. The set-up has been connected to the peristaltic pump for the whole duration of the experiment in order to maintain the capillary velocity of the fluid inside.

5.3.4. Cell picking

Cell passage from the gel (primary tumor) to the fluidic circuit, and from this to the metastatic chamber, was monitored by removing and replacing the medium every 24 hours for a total of 2 days. As early as the first 24 hours, both single and cluster cells were detected both in the primary and in the metastatic circuit, confirming that they are able to migrate through the porosity of the membranes (Fig. 4, panels A and B). Some cells were aspirated by applying suction to the capillary micropipette; the CellCelector software documents each cell picking process by taking an image from the picking area before, during and after picking the cell (Fig. 4, panels C to E).

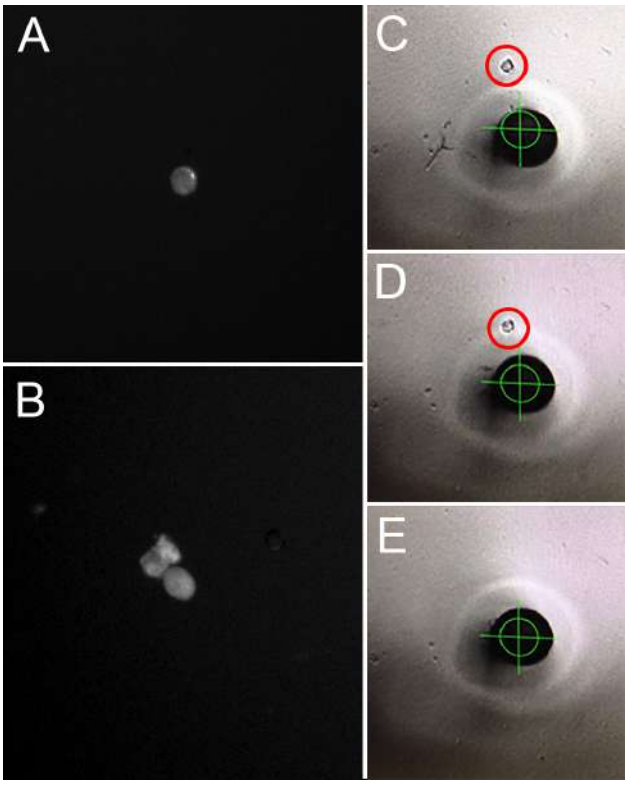

Figure 5.4: A) Single LM2 observed in circulation after 24 hours. B) Cluster of two LM2 cells observed in circulation after 24 hours. C-D-E) Sequence of cell picking process: a single cell (red circle) is aspirated by the glass capillary of CellCelector.

5.3.5. Cell counting

Number of intravasated/extravasated cells (cells passed into the main and the metastatic circuit, respectively) was monitored up to 48 hours and converted to percentage respect to the initial amount of cells. Figure 5, panel A shows that an average of 0.1% was found in the main circuit after one day, while 0.01% was found at the same time into the metastatic chamber. After 48 hours from the beginning of the experiment, quantities increased to 0.51% and 0.1% into the main and metastatic circuits, respectively.

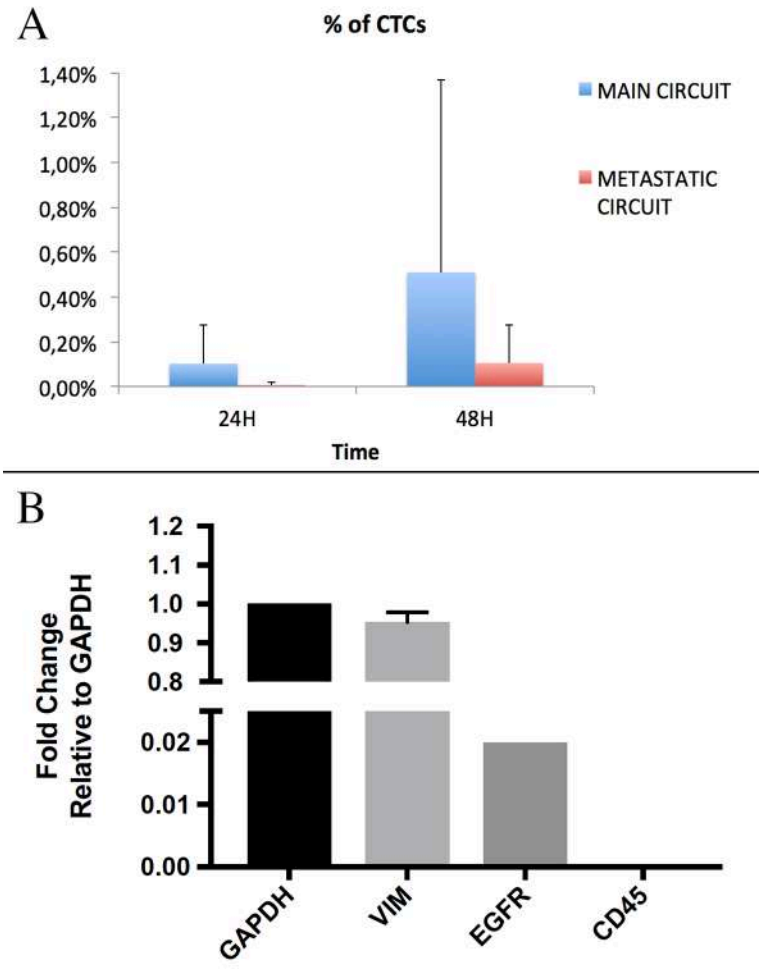

Figure 5.5: - A) Counting of CTCs found in the main and metastatic circuits after 24 hours and 48 hours. Counting is expressed as percentage of the number of cells seeded within the gel. B) Expression of GAPDH, Vimentin and EGFR (all three well established markers of LM2) and CD45 (negative control, white blood cell marker) of a circulating LM2.

We know from literature that a tumor reaching the size of 1 cm3 (approximately 1 g wet weight) is commonly assumed to contain 1 x 109 cells. However, mostly in epithelial tumors (such as breast cancer), a cell number one order of magnitude smaller (108 cells) would be more realistic[40]. We also know that circulating tumor cells (CTCs) are a fundamental

prerequisite to metastasis. Most clinical studies, so far, have focused on CTC enumeration in guiding prognosis in metastatic cancer patients and current research is exploring the pharmacodynamics and predictive biomarker utility of CTCs. In breast cancer, a quantity of CTCs ≥5 into 7.5 ml (0.7 CTCs/ml) is considered as an independent predictor for poor outcome in terms of progression-free survival[41].

Considering that an average adult has about 5 liters of blood circulating inside their body, 0.7 CTCs/ml means 3500 CTCs that, respect to a tumor composed by 108 cells, is the 0,0035%.

Our percentages, although higher than those found in reality, show a similar trend. The differences can be traced back to the absence of the immune system in the in vitro system and, in general, to the preliminary phase of the study, which however results very promising.

5.3.6. RNA analysis

Single cell qPCR of the circulating LM2 cells was performed. The vast majority of cells gave no signal (this could be due to poor fitness of the cells): this is another remarkable result of the study, since preclinical models demonstrate that within 24 hours of intravenous administration of tumour cells, less than 0.1% cells remain viable and that less than 0.01% of these surviving CTCs can produce metastasis[41]. On the other side, other cells showed very good data. As example, a single LM2 circulating cell is reported: in this cell, we detected GAPDH, Vimentin and EGFR (all three well established markers of LM2) but not CD45 (white blood cell marker). This provides a proof-of-concept that the approach can work, as well as evidence

that the cells can be extracted from the device and used for molecular analysis.

5.4. References

1 Fong, E. L., Santoro, M., Farach-Carson, M. C., Kasper, F. K. & Mikos, A. G. Tissue engineering perfusable cancer models. *Current opinion in chemical engineering* **3**, 112-117 (2014).

2 Hirt, C. *et al*. Bioreactor-engineered cancer tissue-like structures mimic phenotypes, gene expression profiles and drug resistance patterns observed "in vivo". *Biomaterials* (2015).

3 Wendt, D., Jakob, M. & Martin, I. Bioreactor-based engineering of osteochondral grafts: from model systems to tissue manufacturing. *Journal of bioscience and bioengineering* **100**, 489-494 (2005).

4 Orr, D. E. & Burg, K. J. L. Design of a modular bioreactor to incorporate both perfusion flow and hydrostatic compression for tissue engineering applications. *Annals of biomedical engineering* **36**, 1228-1241 (2008).

5 Beachley, V. & Wen, X. Effect of electrospinning parameters on the nanofiber diameter and length. *Materials Science and Engineering: C* **29**, 663-668 (2009).

6 Khil, M. S., Cha, D. I., Kim, H. Y., Kim, I. S. & Bhattarai, N. Electrospun nanofibrous polyurethane membrane as wound dressing. *Journal of Biomedical Materials Research Part B: Applied Biomaterials* **67**, 675-679 (2003).

7 Deitzel, J. M., Kleinmeyer, J., Harris, D. E. A. & Tan, N. C. B. The effect of processing variables on the morphology of electrospun nanofibers and textiles. *Polymer* **42**, 261-272 (2001).

8 Doerr, M. E. & Jones, J. I. The roles of integrins and extracellular matrix proteins in the insulin-like growth factor I-stimulated chemotaxis of human breast cancer cells. *Journal of Biological Chemistry* **271**, 2443-2447 (1996).

9 Del Monte, U. Does the cell number 109 still really fit one gram of tumor tissue? *Cell Cycle* **8**, 505-506 (2009).

10 Krebs, M. G., Hou, J.-M., Ward, T. H., Blackhall, F. H. & Dive, C. Circulating tumour cells: their utility in cancer management and predicting outcomes. *Therapeutic advances in medical oncology* **2**, 351-365 (2010).

11 Jeon, J. S., Zervantonakis, I. K., Chung, S., Kamm, R. D. & Charest, J. L. In vitro model of tumor cell extravasation. *PloS one* **8**, e56910 (2013).

12 Ma, J. & Jemal, A. in *Breast Cancer Metastasis and Drug Resistance* 1-18 (Springer, 2013).

13 Bussard, K. M., Gay, C. V. & Mastro, A. M. The bone microenvironment in metastasis; what is special about bone? *Cancer and Metastasis Reviews* **27**, 41-55 (2008).

14 Zaman, M. H. The role of engineering approaches in analysing cancer invasion and metastasis. *Nature Reviews Cancer* **13**, 596-603 (2013).

Chapter 6

Discussion

It is an established fact that 3D cultures are essential for a better comprehension of cell behaviour, as they recapitulate an environment more similar to the in vivo one. This is particularly important in pathological conditions, such as in cancer studies (e.g. breast cancer, the most common tumour in women), offering alternative approaches for the testing of new drugs; however, at the moment no established 3D models with clinically relevant size and features exist to carry out standardized and reproducible studies on breast cancer and, most importantly, on its metastatic spread.

The availability of 3D models offering the appropriate in vitro microenvironment for cell tumour growth is essential to improve our knowledge of cancer biology and successfully test new anticancer compounds: animal models have proven to be not entirely compatible with the human system, and the success rate between animal and human studies is still unsatisfactory. On the other hand, 2D cell cultures are useful tools for cancer studies but they fail to reproduce some crucial aspects of tumours, such as 3D cell growth and cell-matrix interactions. These limitations have a significant weight especially during the screening of novel drugs, since it has been demonstrated that cells become less sensitive to anti-cancer treatments when in contact with their microenvironment.

Thus, to obtain the same cancer cell inhibition level observed in vivo, the culture environment has to reflect the 3D natural environment, including its mechanical cues. Indeed, the biochemical (e.g. adhesiveness) and physical

properties (e.g. substrate stiffness) of the extracellular microenvironment have been recognized as independent factors that influence cell function and tissue morphogenesis in multiple ways41. Consequently, both categories must be considered when designing substrates for cell culture applications.

In this context, the field of tissue engineering (TE) offers powerful tools to achieve 3D in vitro cancer models that are representative of in vivo solid tumours. Some TE-based cancer models have already been proposed, showing promising results in recapitulating several aspects of tumour microenvironment complexity16. Above all, natural or synthetic hydrogels reported successful outcomes in mimicking the ECM environment, thanks to their high water content and remarkable biocompatibility. In particular, Collagen I-based hydrogels showed promising angiogenic potential with a significant up-regulation of vascular endothelial growth factor (VEGF) gene expression, representative of the pre-vascularized stages of in vivo solid tumour progression42. Laminin-rich gels were adopted and validated as 3D platforms able to distinguish non-malignant versus malignant breast cells: when embedded in such gels, the non-malignant cells were organized into polarized colonies similar to mammary acini, while malignant cells lost cell polarity and underwent the disorganized growth typical of in vivo tumours43.

However, in these studies, the tentative of reproducing the chemical features of the native ECM made the investigation of cell response to mechanical stimuli (mechano-responses) more complicated44.

In the first work presented in this thesis (**Chapter 3**), I have realized and characterized 3D alginate-based hydrogels. Although alginate has already been demonstrated to be an excellent substrate for breast cancer cell culture45, I stressed the physical properties of alginate gels, including their stiffness, with the final aim of studying the effect of substrate elasticity on breast cancer cell activity (i.e. viability, proliferation and cluster formation). Alginate serves as a model, since its properties reflect those of many other gels. The following considerations, however, can be applied to

other polymers, being independent from the chemical properties of the substrates. The first step of this work was dedicated to definition of the parameters (Alginate percentage and cross-linker CaCl2 content) capable of modulating gel stiffness, quantified as elastic modulus. Among the techniques and laboratory instruments typically used for the mechanical characterization of 3D substrates, Atomic Force Microscopy (AFM) was chosen, since it allows measurement of hydrogel stiffness with a size-scale comparable to the cellular one, for a better understanding of the cell-substrate stiffness interaction. Human breast cancer cells (MCF-7) were directly embedded within alginate gels with different elasticity, and cultured for up to 14 days. Cellular viability and cytoskeleton morphology were evaluated at early time points, since they are mostly a biological response to a specific event/environmental condition, e.g. substrate stiffness, chemical structure (plastic vs. alginate) and complexity (2D vs. 3D). Cell proliferation and cluster formation were analysed at both 7 and 14 days, in order to evaluate the progressive evolution of these processes within alginate-based gels. Remarkably, my results show that stiffness directly influences cells fate, not only in a 2D culture set-up as already demonstrated, but also in a more realistic 3D microenvironment where we observed a proportional elasticity-mediated cellular viability. In particular, I found that MCF-7s consistently proliferated in gels characterized by elastic moduli ranging between 150–200 kPa, until cell clusters of 100 μm- and 300 μm-diameters were obtained after 1 and 2 weeks, respectively. This uninhibited proliferative capacity, hereby observed in the softest gels, is one of the key stages that identifies the initial pre-vascularization and growth of solid tumours40,46. Additionally, the multicellular, cluster-like, conformation observed in 3D gels was much closer to in vivo solid tumour organization than the one seen in both 2D Petri and 2D-alginate cultures, thus demonstrating the benefit of 3D cancer models for reproducing cell-cell and cell-matrix interactions47,48. As a consequence, I suggest that cellular morphology may be strongly affected by microenvironment dimensionality: tumour cells showed a flat morphology when expanded in 2D cultures, where only a segment of the cell membrane can interact with

the substrate, while they exhibited a round shape in the 3D environment. In this condition, their proliferation strictly depends on substrate stiffness, which may affect the diffusion of nutrients and intracellular signalling through a mechano-transduction mechanism.

Although the proposed in vitro breast cancer model specifically addresses the evaluation of cellular response to different substrate elasticity ranges and avoids the overall complex nature of the tumour microenvironment, some key characteristics of breast tumours, such as cluster organization and cellular morphology, have been successfully reproduced here. Therefore, it is desirable and expected that such a model could be enriched with further features (e.g. chemical and biological functionalization) to better emulate in vitro the natural tumour niche. These advanced models could be finally used for initial therapeutic screenings, e.g. evaluating if the administration of anticancer agents causes cell apoptosis or breaks cell proliferation as observed in successful in vivo chemotherapy treatments.

In the work presented in **Chapter 4**, I presented new 3D models of highly aggressive breast cancer, allowing cells expressing some features characteristic of their aggressiveness and manifesting that capacity of motility at the base of the metastatic cascade. Invasiveness assays usually adopt a thin layer of reconstituted Matrigel in Boyden chambers as very rapid, easy and inexpensive test that can be used to detect the migratory activity associated with matrix degradation and quantify the invasive potential of cells [42]. Because of the rapid degradation of Matrigel, this assay usually lasts few hours and Matrigel can't be used as 3D substrate maintaining cells entrapped in.

From these starting considerations, the idea of new composites able to join the advantages of the two bulk materials was born, with the final aim to obtain a structurally performing and biologically permissive material to be used as

standard model for the 3D culture of aggressive breast cancer cells and for testing chemotherapeutic agents in vitro.

To accomplish this, I first designed five different hydrogel compositions (i.e. 100% A, 75%:25% A:M, 50%:50% A:M, 25%:75% A:M, 100% M), finally excluding 25%:75% A:M and 100% M because of a weak structural robustness and a low resistance in culture during the 7 days of culture. The remaining three categories were validated from a biological point of view, firstly assessing cell viability and proliferation both within the outer and inner parts of gels. Results show that cells were able to proliferate up to 4 times in all gel types; although cells within gels do not experience the same adhesion they have in 2D, it is known that tumour cells, and in particular MDA-MB-231 cells, are resistance to anoikis[43]. The sight difference subsisting in favour of alginate substrates may be attributed to the capability of cancer cells to easily migrate within the Matrigel and thus to more easily escape from Matrigel-based gels. Confocal microscopy tools and 3D reconstruction techniques were used to analyse the morphological features of the cells, highlighting those differences related to their malignancy.

I observed that cells maintained a spherical shape in 100% A gels, while they assumed elongated shape in presence of Matrigel; this last feature is in agreement with what is known in literature, according to which MDA-MB-231 cells assume a particular stellate shape related to their malignancy. Cell elongation and cytoskeletal irregularity proportionally increased with the amount of Matrigel in the gels. In 50%:50% A:M gels, irregularity of the cytoskeleton is enhanced by the formation of invadopodia, actin-based protrusion of the plasma membrane through which cells anchor to the

extracellular matrix and degrade it. Remarkably, invadopodia was for the first time observed in a 3D *in vitro* model. Cell nuclei expressed irregular shape and poly-nuclei organization exclusively in cells with elongated shape and proportionally to the amount of Matrigel. This feature is known to be linked to cell malignancy as well, allowing us to say that 50%:50% A:M gels allow MDA-MB-231 cells to express those typical features of their aggressive *in vivo* behaviour.

Finally, a bioreactor-based set-up for cell intravasation was adopted to monitor cell ability to migrate out from the gels. My results show that both in 75%:25% A:M and in 50%:50% A:M cells were able to migrate through the gels, escape from them and adhere to a porous electrospun membrane functionalized with gelatine to promote cell attachment.

These data, combined together, allows to say that a new 3D model of aggressive breast cancer (i.e. 50%:50% A:M) was provided. It is based on an hydrogel-based, 3D, culture method which allows human carcinomas to grow *in vitro* and to maintain many typical *in vivo* properties, including 3D architecture, poly-nuclei and invadopodia manifestation, expression of morphological differentiation and migration capability. Since we observed migration specifically into Matrigel containing networks, my data further suggest that cells interact actively with the matrix during dissemination.

If a close mimicry of the *in vivo* situation is desired, it should be taken into account that tumours are 3D, auto-consistent structures and that metastatic cells actively escape from the primary tumour before entering in circulation. For this reason, standard microfluidic platforms and organ-on-chip

technologies, usually using free circulating cancer cells, are poorly representative of the human context.

In conclusion, this 3D cell-laden hydrogel, combined with the presented bioreactor technology, is a good compromise between a reflection of the *in vivo* situation and manageable experimental effort, finally providing a revolutionary approach for studies on invasive breast cancer and drug testing.

Finally, in **Chapter 5** I focused on a new set-up for the observation of cancer cell motility and invasion. In particular, I combined a bioreactor-based bioengineering approach with single cell analysis of Circulating Tumor Cells (CTCs). Analysis of human CTCs has now revealed important features of cancer metastasis, such as the high metastatic potential of CTC-clusters compared to single CTCs, the dynamic expression of epithelial and mesenchymal markers on CTCs during treatment, and the possibility to culture CTCs from patients for a real-time and individualized testing of drug susceptibility. Nevertheless, several aspects of CTC biology remain unsolved, such as the characterization of the stem-like cell population among human CTCs. Defining the molecular features of those few metastasis-initiating, stem-like CTCs holds the exceptional promise to develop metastasis-tailored therapies for patients with cancer.

For this reason, I applied the same approach to my in vitro system. Single cell qPCR of the circulating LM2 cells was performed. The vast majority of cells gave no signal (this could be due to poor fitness of the cells): this is another remarkable result of the study, since preclinical models demonstrate that within 24 hours of intravenous administration of tumour cells, less than 0.1%

cells remain viable and that less than 0.01% of these surviving CTCs can produce metastasis[41]. On the other side, other cells showed very good data. As example, a single LM2 circulating cell is reported: in this cell, we detected GAPDH, Vimentin and EGFR (all three well established markers of LM2) but not CD45 (white blood cell marker). This provides a proof-of-concept that the approach can work, as well as evidence that the cells can be extracted from the device and used for molecular analysis.

List of publications

International peer-reviewed papers

1. **Cavo M.** and Scaglione S. - Scaffold microstructure effects on functional and mechanical performance: integration of theoretical and experimental approaches for bone tissue engineering applications. **Materials science and engineering C**, July 2016 (IF: 3.420)
2. Zamuner A., **Cavo M.**, Scaglione S., Messina G.M.L., Russo T., Gloria A., Marletta G. and Dettin M. - Design of decorated self-assembling peptide hydrogels as architecture for mesenchymal stem cells. **Materials**, August 2016 (IF: 2.728)
3. **Cavo M.**, Fato M., Peñuela L., Beltrame F., Raiteri R. and Scaglione S., "Microenvironment complexity and matrix stiffness regulate breast cancer cell activity in a 3D in vitro model". **Scientific Reports**, September 2016 (IF: 5.228)
4. **Cavo M.**, Caria M., Beltrame F., Fato M., Scaglione S. - A new cell laden 3D Alginate-Matrigel hydrogel resembles human breast cancer cell malignant morphology, spread and invasion capability observed "in vivo", submitted
5. **Cavo M.**, Di Maggio N., Szcerba B., Krol I., Fato M., Aceto N., Scaglione S. - A novel fluid-dynamic and multi-organ bioreactor combined with single cell picking allows recapitulating the metastasis paradigm in vitro (in preparation).

Contributions to books

1. Marrella A., **Cavo M.** and Scaglione S., "Rapid prototyping for the engineering of osteochondral tissues". Chapter within the book “Regenerative strategies for the treatment of Knee Joint disabilities" editor by Springer, January 2017

Oral presentations at international and national congresses

1. **Cavo M.**, Fato M., Beltrame F. and Scaglione S., "Matrix stiffness regulate breast cancer cells activity in a 3D in vitro model", European Society of Biomechanics (ESB) conference, July 10th-13th 2016, Lyon (France).
2. Scaglione S., Marrella A. and **Cavo M.**, "Bioactive scaffolds for articular tissue engineering applications", AIMETA XXII Congresso - Associazione Italiana di Meccanica Teorica e Applicata - September 14th-17th 2015, Genoa (Italy).
3. **Cavo M.**, Fato M., Coluccino L., Beltrame F. and Scaglione S., "Development of 3D alginate-based hydrogels with different mechanical properties as in vitro breast cancer model", AIV XXII conference – May 22nd 2015, Genoa (Italy).

Posters

1. **Cavo M.**, Fato M., Marrella A., Beltrame F. and Scaglione S., "Mechanically-tuned alginate gels as new 3D breast cancer models", Tissue Engineering and Regenerative Medicine International Society (TERMIS) european conference - June 28th-July 1st 2016, Uppsala (Sweden).
2. **Cavo M.**, Fato M., Beltrame F. and Scaglione S., "Mechanically-tuned alginate gels as new 3D breast cancer models", Bioengineering National Group (GNB) V congress - June 20th-22nd 2016, Naples (Italy).
3. **Cavo M.**, Fato M., Beltrame F. and Scaglione S., "Importance of matrix stiffness in realizing 3D in vitro breast cancer models", Enabling technologies in 3D cancer organoids Workshop - March 8th-9th 2016, Turin (Italy).